CLIQUES CAN CLICK! EVOLUTIONARY DYNAMICS ON TWO-CLIQUE AND CLIQUE-LIKE GRAPHS WITH RESOURCE HETEROGENEITY

A Thesis

Submitted to the Faculty

in partial fulfillment of the requirements for the

degree of

Bachelor of Arts

in

Mathematics

by

Archita Harathi

DARTMOUTH COLLEGE

Hanover, New Hampshire

May 2022

Abstract

The evolutionary dynamics of a finite population can be modeled on graphs, where individuals inhabit graph nodes and competing types reproduce, migrate, and die. We explore the dynamics of the Moran process, where a mutant type and a resident type compete for fixation influenced by their reproductive advantages. Previous literature has explored how characteristics of graphs can affect the likelihood of mutant success. In particular, related research explores graph structure, which influences offspring migration, and graph coloring, which models environmental impacts on reproduction. We expand on this work by evaluating mutant fixation on two-colored two-clique and clique-like graphs, representing connected islands of nodes with high-quality resources and low-quality resources. This thesis explores how increasing connectivity between and within these islands, varying island sizes, changing fitness heterogeneity for both types, and modeling resource depletion impact the fixation probability of a mutant type. Firstly, we find that as environmental variability increases, increasing clique inter-connectivity typically decreases fixation probability. Secondly, we show that increasing the relative size of low-quality resource cliques increases fixation probability. Thirdly, we find that fixation probability is generally highest when residents but not mutants are susceptible to environmental heterogeneity. Lastly, we conclude that resource depletion can actually improve mutant success rates. Overall, mutants perform better with cliques–specifically those that have fewer inter-connections, more poor-quality nodes, less environmental variation, and more resource degradation.

Acknowledgements

Thank you to my advisors Professor Feng Fu and Professor Kamran Kaveh for the guidance, advice, and support throughout my mathematics education and the thesis writing process. I also appreciate the support of the Department of Mathematics at Dartmouth College for providing me with opportunities to learn, grow, and think math. Thank you to Matt Sawicki for being my project partner in my mathematics culminating experience at Dartmouth, which is where my exploration of this field began. I also want to emphasize my appreciation for my high school education and my high school math teacher Dr. John Gorman who showed me how beautiful and challenging mathematics could be, inspiring me to continue pursuing math in college. Thank you to all of my friends for their support and curiosity in my interests. Lastly, but surely not least, thank you to my parents and my brother for their encouragement, love, and care throughout my life–I would not be anywhere near as excited about my education and passions without them.

Contents

Chapter 1

Introduction

Section 1.1

Evolutionary Dynamics on Graphs

The study of evolutionary dynamics explores the interaction and success of various strategies or types within a reproducing population [1, 11]. Evolutionary processes are influenced by reproduction, the production of offspring, mutation, or the creation of new (potentially favorable or unfavorable) types, and selection, or the survival of a type based on its reproductive success [2, 14, 25]. These processes are also very much influenced by randomness [17]; in addition to intrinsic differences in the reproduction of different types, environmental variations influence how these evolutionary interactions occur [27]. We study how reproductive, spatial, and environmental differences characterize and impact evolutionary interactions.

1.1.1. Moran Process

We explore in this paper the likelihood of survival of a mutant type in a finite population. There are two commonly known stochastic processes for evolutionary dynamics: the Moran process and the Fisher-Wright process [27]. The former process involves a

single individual giving birth at each time period, allowing individuals to survive for multiple generations, while the latter involves simultaneous births of all individuals resulting in a completely new generation at each time step [26, 27]. To model our exploration of mutant survival in this paper, we use the Birth-death Moran process to simulate the birth and death of individuals over time. A more detailed description of the Moran process is as follows.

Take a population of size N, comprised of N_A individuals of type A, or mutant individuals, and N_B individuals of type B, or resident individuals [25, 27]. The two types could represent any pair of competing groups, such as alleles or phenotypes [5]. We start with 1 individual of type A and $N-1$ individuals of type B [9], as an important question in evolutionary dynamics asks what occurs following the inception of a mutant [3]. In the simplest Birth-death Moran process, at each time step t, one individual is randomly chosen to reproduce and one individual is randomly chosen to die [25]. The total population size remains constant, and either type A gains an individual and type B loses one, type B gains one and type A loses one, or the population sizes of both types A and B remain the same.

In the non-neutral Birth-death Moran process, we assume that individuals of type A have a reproductive rate of $r_a = r > 1$ and that individuals of type B reproduce at a rate of $r_b = 1$, so individuals of type A have an advantage in selection [25]. In this case, an individual is chosen to reproduce based on its relative fitness, and once this reproduction occurs, a random individual is chosen to die [25]. Given i mutants in the population, the probability that the number of mutants increases is [9]

$$p_{i,i+1} = \frac{r \cdot i}{r \cdot i + N - i} \cdot \frac{N - i}{N - 1} \tag{1.1}$$

while the probability of decreasing the number of mutants in the population is [9]

$$p_{i,i-1} = \frac{N-i}{r \cdot i + N - i} \cdot \frac{i}{N-1}. \tag{1.2}$$

Typically in some evolutionary process, after long periods of time, only one type survives [29]. In the Moran process, there is no possibility of coexistence between types, and so at a certain time step the process will end in one of the two absorbing states with either 0 or N mutants [25]. This means that $p_{0,1} = p_{N,N-1} = 0$ [6, 9]. With some algebraic manipulation of the above equations, we discern that the probability of a mutant fixating, ρ, in a homogeneous population where all nodes have an equal likelihood of being replaced is equal to [7, 25]

$$\rho = \frac{1 - \frac{1}{r}}{1 - \frac{1}{r^N}}. \tag{1.3}$$

We find that in large finite populations, where $N >> 1$ [25],

$$\rho \approx 1 - \frac{1}{r} \tag{1.4}$$

These equations reveal that population size does not necessarily guarantee fixation or extinction; rather, success in this randomized evolutionary process is influenced by a variety of factors, including the degree to which mutants are reproductively advantageous [25].

Some other forms of update rules include the Death-birth process, in which a random individual is replaced by an individual's offspring, chosen with probability relative to fitness (similar to its reproductive rate), or Imitation, where a random individual dies and its neighbor is chosen reproduce based on its fitness (in this case the offspring can replace its parent) [1]. In this paper, we exclusively focus on the Birth-death Moran process described above.

1.1.2. Graph Theory

The dynamics of the Moran process can be modeled using graphs. In this literature, the vertices of a graph translate to the individuals of a population and weighted edges model dispersal rates that capture how offspring move into nearby vertices [4]. These edges between nodes can be undirected, meaning that adjacent individuals can replace each other, based on the degree of the node and the individual's fitness [10]. Undirected edges represent symmetric interactions between individuals [18], so an edge between vertex i and j denotes that an offspring from vertex i can replace the individual in vertex j and vice versa [25]. While mathematical representations, these graphs can represent real-world biological and ecological phenomena. Evolutionary graphs could describe processes anywhere from cell structure and hierarchy within multi-cellular organisms to social and cultural relations between humans [25].

One particular metric of interest in these graphs is fixation probability, ρ, or the likelihood that a mutant individual will completely overtake the population [4], which is averaged over all states starting with one mutant. This probability influences the rate of evolution [28]. Previous work has shown that the structure of a graph can greatly influence the success of a mutant strategy and evolutionary dynamics [9].

Varying graph structure can represent a variety of real-world phenomena. The spatial arrangement of some ecosystems, like rivers, can influence reproduction and migration of species, similar to how the structure of colonic crypts can impact the growth of cancer cells [22]. For these reasons, to model how natural processes work, we observe how evolutionary dynamics change with various graph structures. The method of observing how spatial structure interacts with evolutionary dynamics has become an important part of mathematical descriptions of evolutionary processes [21].

The Moran process on the complete graph, or a graph with undirected edges be-

tween all nodes, represents evolutionary dynamics on a well-mixed population [13], and is the general comparison baseline for evaluating the fixation probability in certain graph structures [22]. If a graph increases the fixation probability of a mutant compared to that of the complete graph when the mutant is advantageous ($r > 1$) and comparably decreases the fixation probability when the mutant is disadvantageous ($r < 1$), then the graph is an amplifier of selection [22]. Some well-known amplifiers are stars [4], or graphs with one central node of degree $N - 1$, and superstars, or graphs with chains of vertices and a central node with a large out-degree and low in-degree [15]. In fact, Broom et al. show that certain graph structures can increase fixation probability, as stars have the highest fixation probability, followed by star-like graphs, while regular graphs tend to have the lowest likelihood of fixation [19]. In contrast, if the fixation probability on a particular graph structure increases when the mutant is disadvantageous and decreases when the mutant is advantageous, compared to the complete graph, then the graph is a suppressor of selection [22].

Another aspect of the structure of these graphs in evolutionary dynamics is with regards to the isothermal theorem. The theorem states that a large number of graph structures, called isothermal graphs, have fixation probabilities that are the exact same as the fixation probability for the well-mixed population [24]. Previous work in this field also found that the initial graph position of the mutant also matters, as there is a negative relationship between the degree of the inception vertex and the likelihood of fixation [19]. Additionally, there is a positive relationship between the fixation probability of a mutant in a randomly placed node and the diversity of vertex degrees in a graph [20].

Aside from these effects of graph structures and reproductive fitness of types on fixation probability, environmental factors can also influence the success of a mutant type in fixating. For example, ecological variation through the availability of

resources could exert favorable or unfavorable constraints on an individual, affecting their reproductive rate [11]. Known as resource heterogeneity [11], this could impact any and all types within a population, thereby also affecting interactions between the types.

1.1.3. Resource Heterogeneity

Looking at resource heterogeneity and environmental variation allows to further understand a variety of real-world processes. Variation across environments is everywhere– from the varied effectiveness of a drug on cancerous cells, to habitat diversity and its impact on breeding and species reproduction, to how an individual's education and familial environment affect their future salary and success [16].

Current literature explores the impact of resource heterogeneity in graph models of evolutionary dynamics using coloring, where a vertex's color represents the quality of resources it provides [16], or a proxy for the fertility of the individual that resides in the vertex [30]. While the number of colors, or environmental conditions, in a graph can be up to N, where each vertex is a different color, we follow a model with two colors, or two levels of resource quality [11]. Vertices that provide high-quality resources to an individual positively benefit the individual's reproductive fitness, and vertices with low-quality resources are a detriment to an individual's fitness. The difference between the high-quality resource locations and low-quality resource locations translates to the resource heterogeneity of the graph [11]. Current methods in this field assume that the effect of a resource level in an environment on an individual's fitness varies by type; for all types, the resulting change in fitness is proportional to the standard deviation of the reproductive fitness [11].

The resulting fitnesses of types A and B in a resource heterogeneity model can be seen below, where r represents the type's mean fitness, σ represents the standard deviation for the type's fitness, and c_v represents the color c at vertex v, so $c_v = 1$ at

high-quality resource vertices and $c_v = -1$ at low-quality resource vertices [11].

$$f_{a,v} = r_a + \sigma_a \cdot c_v \tag{1.5}$$

$$f_{b,v} = r_b + \sigma_b \cdot c_v \tag{1.6}$$

Four main identifications that result from this model include symmetric interactions, where $\sigma_a = \sigma_b$, also known as background fitness heterogeneity, asymmetric interactions, where $\sigma_a = -\sigma_b$ [11], mutant heterogeneity, where $\sigma_b = 0$, and resident heterogeneity, where $\sigma_a = 0$ [16].

Dynamic environments are also of interest. These situations could translate to high-quality resources and beneficial conditions lessening over time, such as depleting nutrients or worsening climate [16]. Previous literature has found that the likelihood at which these resources "move" can in some cases amplify the effects of heterogeneity on fixation, and in other cases decrease how heterogeneity impacts fixation probability [16].

Section 1.2

Outline

This paper seeks to extend current literature regarding the interplay between resource heterogeneity, graph structure, and fixation probability. We first explore how increasing the connectedness of a graph influences the likelihood of fixation as fitness changes across various environments. We study this increase on the number of connections within *islands* (cliques or clique-like subgraphs) and between islands. Our results reveal that intra-connectivity plays much less of a role on mutant success than inter-connectivity between cliques. We find that increasing the inter-connectedness of

a two-clique or clique-like graph tends to decrease the fixation probability of a single mutant as both type A and type B experiences more variable environments.

We also try to understand how relative sizes of these subgraphs influence fixation probability. We find that while the impacts on fixation probability are slight, mutants do see benefits to two-clique graphs with larger low-quality resource cliques compared to high-quality resource cliques. The trends in inter-connectivity on balanced two-clique graphs are also verified for these unbalanced two-clique graphs.

Consistent with previous literature's exploration of fitness heterogeneity, we also question how varying this fitness heterogeneity model affects fixation probability; that is, how relative fitness deviations between type A and type B individuals influences fixation. For two-clique graphs with less inter-connectivity, we find that background fitness heterogeneity–when mutant types and resident types face the same environmental variation–allows the mutant to perform better the more advantageous they are (when they have a larger mean fitness). However, as inter-connectivity between these cliques increase, other heterogeneity models perform better. Specifically, when only residents face environmental variation, mutants perform best.

Lastly, we explore how dynamic environments affect the fixation probability of a population. We show that incorporating resource depletion actually allows the mutant to succeed more often, and actually helps some graph structures that typically inhibit mutant fixation become structures that aid in mutant fixation.

Chapter 2

Model and Methods

Section 2.1

Two-Clique and Clique-Like Graphs

Previous work in evolutionary graph theory has explored the implications of population structure and resource heterogeneity on fixation probability for a variety of different graphs. For example, Kaveh et al. exactly compute a formula for the fixation probability of biregular, properly-two colored graphs, including bipartite cycles, stars, lattices, and complete graphs [16]. Others have looked at clique-based graphs of one-color, formed by combining cliques with isolated vertices and cycles, and have found graph variations that can change from amplifiers to suppressors [12].

In contrast to properly-two colored or bipartite graphs, where adjacent vertices are different colors, or clique graphs with only nodes of one type, we seek to understand the implications of connections between nodes of *similar* types and *different* types. Forming *islands*, these clusters of similar environments can mimic larger connected regions with similar quality resources, allowing individuals of any type to move freely among nodes with no environmental changes, while being able to travel to different terrain as well. We observe the evolutionary result of increasing the connectivity both

within and between these islands of similar nodes. We characterize these connected islands, or subgraphs, or using the standard graph theoretical definition of a clique. In relation to evolutionary dynamics and resource heterogeneity, we refer to *like-nodes* as vertices that have the exact same color, or represent the same environmental habitat or resource quality level.

Definition 2.1 (Two-Clique Graph)**.** A *clique* of a graph G is a maximal complete subgraph of like-nodes [8]. A *two-clique graph* is a graph G comprised of two cliques, [23], C_1 and C_2, such that $\exists$ at least one $v_1 \in V(C_1)$ and at least one $v_2 \in V(C_2)$ where $(v_1, v_2) \in E(G)$.

In conjunction with using maximal complete subgraphs, as seen in Figure 2.1 a), we expand the graphs we consider by relaxing our notion of two-clique graphs to include two-clique-like graphs, which have cyclic islands instead of completely connected islands. This allows us to observe the effect of intra-connectedness within an island (clique or clique-like subgraph) on a mutant's ability to fixate. Figure 2.1 b) provides examples of graphs that are two-clique-like.

Definition 2.2 (Two-Clique-Like Graph)**.** A subgraph of graph G is *clique-like* if it is a maximal cyclic subgraph of like-nodes. A *two-clique-like graph* is a graph G comprised of two clique-like subgraphs, CL_1 and CL_2, such that $\exists$ some $vl_1 \in V(CL_1)$ and $vl_2 \in V(CL_2)$ where $(vl_1, vl_2) \in E(G)$.

Additionally, as consistent with literature, we focus on graphs with only two colors, each coloring one clique. Subsequently, we color low quality resource nodes *red*, and high quality resource nodes *green*. In addition to varying the amount of connections within these red and green cyclic and complete subgraphs, we also explore how increasing the number of inter-connectedness, or adjacencies between islands, can impact fixation probability. In Figure 2.2, we display a number of common graphs

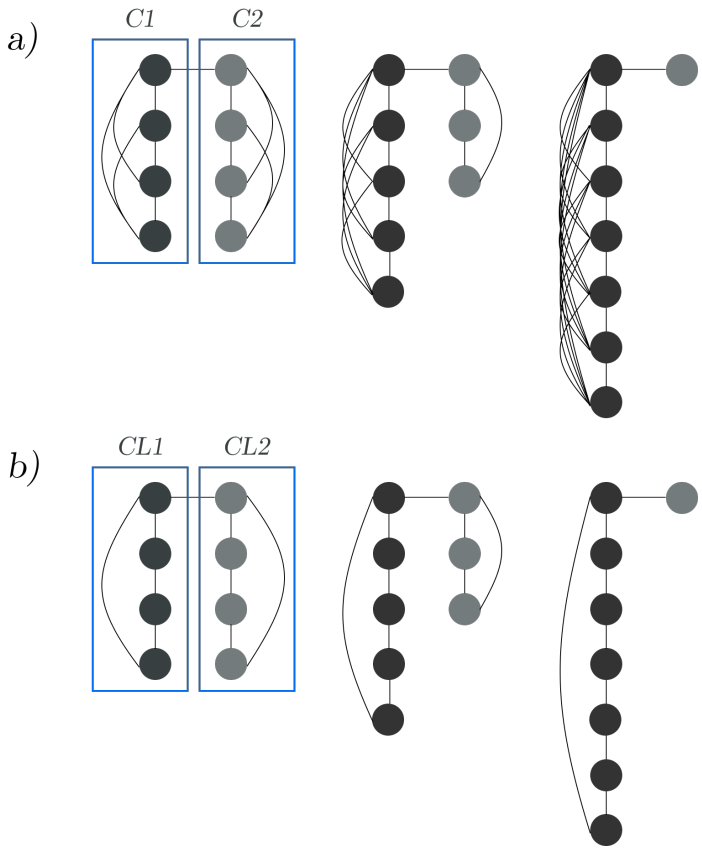

Figure 2.1: Two-Clique and Clique-Like Graph Examples

Part a) provides examples of balanced (left-most) and unbalanced two-clique graphs. The two shades of grey represent different node types, and the complete subgraphs of each type of node form cliques. Part b) provides examples balanced (left-most) and unbalanced two-clique-like graphs.

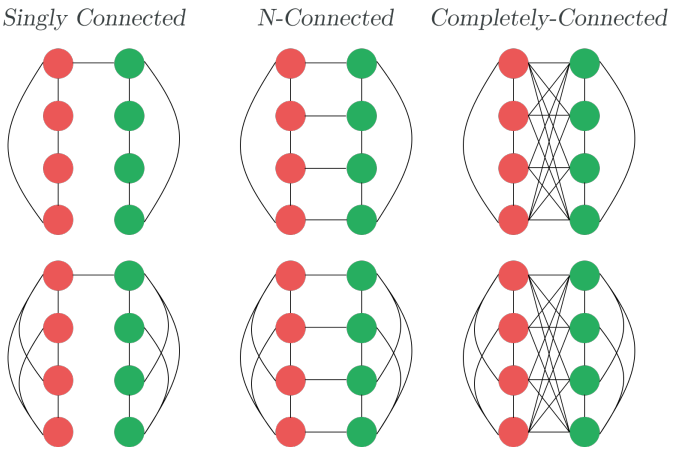

Figure 2.2: Common Two-Clique and Clique-Like Two-Colored Graph Examples

Three different classifications of graphs are shown here, which capture the spread of intra-connectivity and inter-connectivity that we explore in this paper.

that we explore in this paper, along with associated names that we use to describe them. In these graphs and others that we initially explore, unless otherwise specified, we focus on the background heterogeneity fitness model, where mutant and resident types experience the same environmental fluctuations (σ).

Section 2.2

Algebraic Approach & Algorithm

In order to calculate fixation probabilities given a graph structure, coloring, and fitnesses for each type in the population, or $\rho(G, C, r, \sigma)$, we utilize two approaches: an algebraic approach to numerically compute exact fixation probability, and a simulated approach averaged across multiple runs until mutant fixation or extinction. The algebraic approach is as follows.

Following the method outlined by Hindersin and Traulsen (2014), we find the transition matrix $T_{s \times s}$ of the Markov chain of the Moran process graph states, where t is the number of transient states of the model, a is the number of absorbing

states, and $s = t + a$ is the total number of states [9]. In the case of the Moran process, we have that $a = 2$. The matrix $T_s \times s$ is comprised as follows, where $Q_t \times t$ captures the transition probabilities between transient states and $R_t \times a$ captures the transition probabilities from transient to absorbing states [9].

$$T_s \times s = \begin{pmatrix} Q_t \times t & R_t \times a \\ 0_a \times t & I_a \times a \end{pmatrix} \tag{2.1}$$

We compute the fundamental matrix of the Markov chain, F, by

$$F_t \times t = (I - Q)^{-1} \tag{2.2}$$

and then compute, Φ, which calculates the absorption probabilities based on the expected time spent in transition states given by F and the probabilities from transition to absorbing states given by R [9].

$$\Phi_t \times a = F_t \times t \cdot R_t \times a \tag{2.3}$$

The i, j-th entry of Φ is the probability of arriving to absorbing state j from transient state i [9]. In our model, fixation probability, ρ, is defined as the average of the absorption probabilities for each i transient state starting with one single mutant and transitioning to the absorbing state m with all mutants.

$$\rho = \frac{\sum_{i=1}^{n} \Phi_{i,m}}{n} \tag{2.4}$$

We provide an example of the calculation of this transition matrix of the Markov chain Moran process using a cycle graph with $N = 4$ [9], with the states as shown in Figure 2.3. Because any node can contain a mutant or resident type, there are in total 2^N possible graph states. However, the symmetry of the cycle greatly reduces

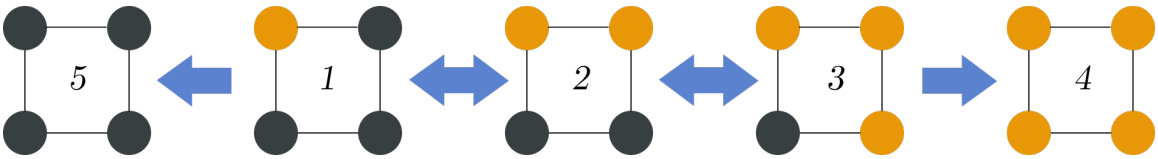

Figure 2.3: Transient and Absorbing States for 4-Node Cycle

The five states above represent the unique graph states for a cycle of four nodes. While there are $2^4 = 16$ possible states, due to the symmetry of the cycle, there are only three transient and two absorbing states. It can be seen in the figure that states 4 and 5 and absorbing states, since they do not transition to any other state but themselves.

the number of transient states we need to consider. Assuming that the fitnesses $f_a = r$ and $f_b = 1$, the transition matrix is provided below.

$$T_{5 \times 5} = \begin{pmatrix} \frac{2}{r+3} & \frac{r}{r+3} & 0 & 0 & \frac{1}{r+3} \\ \frac{1}{2(r+1)} & \frac{1}{2} & \frac{r}{2(r+1)} & 0 & 0 \\ 0 & \frac{1}{3r+1} & \frac{r}{3r+1} & \frac{2r}{3r+1} & 0 \\ 0 & 0 & 0 & 1 & 0 \\ 0 & 0 & 0 & 0 & 1 \end{pmatrix} \tag{2.5}$$

.

Here, the mutant type is represented by the orange nodes, and the resident type is represented by black nodes. In the above matrix, each row i represents a state, s_t in Figure 2.3, and each column j represents s_{t+1}, the state at the next time step, so the resulting ij-th entry corresponds to the transition probability between s_t and s_{t+1}.

We turn to the application of this approach on larger graphs, specifically related to the two-clique and clique-like two-colored graphs of interest in our paper. Figure 2.4 illustrates the number of transition states to be considered for a singly-connected two-clique graph with two colors, represented the the shading of the black (resident) and

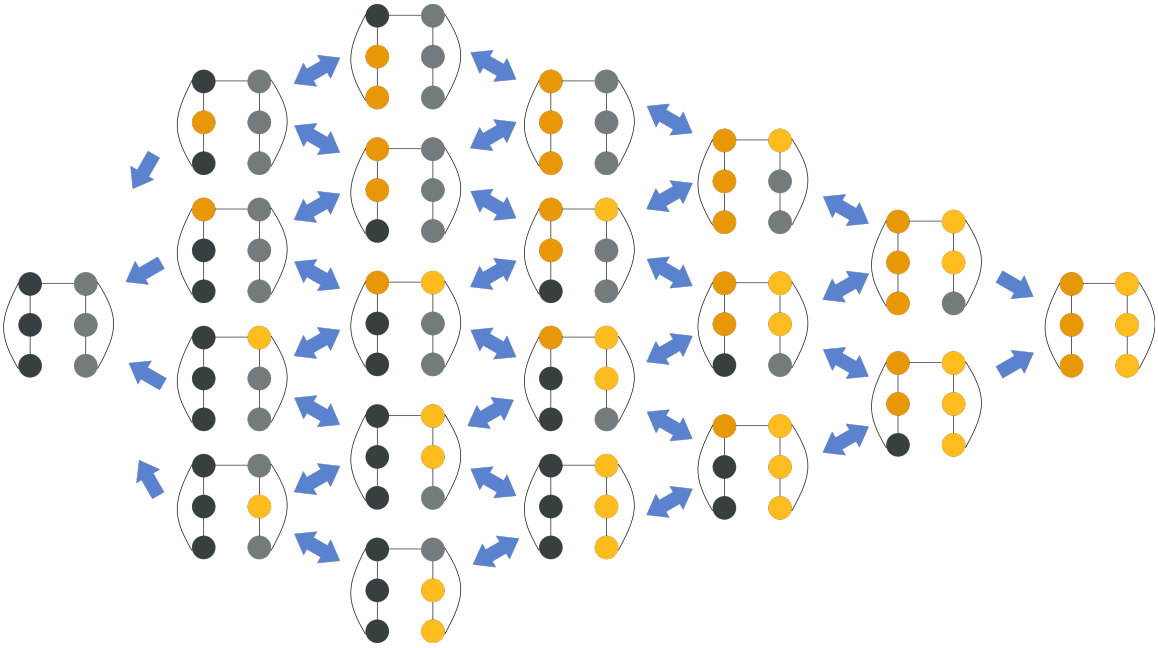

Figure 2.4: Transient and Absorbing States for Singly-Connected Two-Clique 6-Node Graph

The figure displays the 20 unique states for the singly-connected two-clique graph. Although the graph has two colors, or node-types, which could reduce the number of potential symmetries in graph states, there still remains symmetry between the non-singly-connected nodes in the clique subgraphs. Due to the exponential nature of the number of these graph states, an algorithm was created to generalize for all graphs with and without symmetries by looking at each of the 2^N states.

orange (mutant) nodes. While there are not, in this case, 2^6 states to be considered, the exponential possibility of the number of transition states led us to create an algorithm for computational efficiency and generalizability in solving for transition matrices and consequently the fixation probability of any graph.

2.2.1. The Algorithm

The overall premise of the algorithm is as follows.

- Initialize a graph, encoding all 2^N graph permutations of individual positions as binary strings.
- Find the next possible graph states for each graph state.
- Calculate probabilities of transitioning ($T_{S \times S}$) from any state of the graph to any other state of the graph using adjacent vertices and vertex fitnesses.
- Perform the Hindersin & Traulsen calculations to find $\rho = \frac{\sum_{i=1}^{n} \Phi_{i,m}}{n}$ for all n transient states starting with one single mutant and transitioning to the absorbing state m with all mutants.

The pseudocode in the following written algorithm captures the general encoding of a graph as a binary state and a return of the transition matrix, which is used to compute fixation probabilities.

Section 2.3

Simulation Approach

Another method of solving for fixation probability does not include exact numerical computational results, but instead simulates the Moran process over thousands of runs. The approach we use is the Monte Carlo algorithm. This type of algorithm

Algorithm Transition Probabilities

$a \leftarrow$ Vertex Adjacency Dictionary
$b \leftarrow$ Adjacency Binary States Dictionary
$c \leftarrow$ Transition Matrix

procedure Get Adjacent Graph States(a)
  for $state = 1, 2, \ldots 2^{size(a)}$ **do**
    Convert *state* into binary number string *bstate*
    while $index < length(bstate)$ **do**
      Neighbor 1 $\leftarrow$ Replace *index* in *bstate* with 0
      Neighbor 2 $\leftarrow$ Replace *index* in *bstate* with 1
      $b \leftarrow$ Neighbor 1, Neighbor 2
    end while
  end for
  return b
end procedure

procedure Calculate Fitness($vertex$)
  if *vertex* has mutant **then**
    if *vertex* is red **then**
      return 1 - σ
    end if
    return $1 + \sigma$
  else
    if *vertex* is red **then**
      return r - σ
    end if
    return $r + \sigma$
  end if
end procedure

procedure Find Transition Probability($frombstate, tobstate$)
  Find the vertex where a mutant or a resident is added from $frombstate$ to *tobstate*
  Find all neighboring vertices S that also could produce an offspring of that type
  $d \leftarrow$ Neighbor Vertex Fitness Sum
  $e \leftarrow$ Total Vertex Fitness Sum
  for *neighbornode* in S **do**
    $d \leftarrow d + \frac{\text{Calculate Fitness}(neighbornode)}{degree(neighbornode)}$
  end for
  while $node < length(fromstate)$ **do**
    $e \leftarrow e +$ Calculate Fitness($neighbornode$)
  end while
  return $\frac{d}{e}$
end procedure

Algorithm Transition Probabilities

```
procedure Create Transition Matrix(b)
    for bstate1 from 1 ... 2^size(a) do
        for bstate2 from 1 ... 2^size(a) do
            if (bstate1, bstate2) in b then
                c ← Find Transition Probability(bstate1, bstate2)
            else
                c ← 0
            end if
        end for
    end for
    return c
end procedure
```

uses the statistical output from these runs to estimate fixation probability [18]. The steps of the simulation algorithm follow:

- Initialize a state vector of the graph $\vec{n}$ of length N, for N individuals. $\vec{n}_i = 0$ if there is a resident at node i and $\vec{n}_i = 1$ if there is a mutant at node i.
- Choose a vertex for initial mutant at $t = 0$.
- Until an absorbing state is reached, pick a random number x at each time step.
- Calculate the cumulative sum of fitnesses and find the first site i such that $x >$ Cumulative Sum(i). This node i will be the node that reproduces in the time step.
- Randomly pick a node j neighboring i to receive the mutant or resident offspring at node i, so $\vec{n}_j = \vec{n}_i$.
- Once an absorbing state is reached, rerun (approx. 50,000 times).
- Report the fixation probability by finding the share of runs that led to mutant fixation out of all runs that led to mutant fixation or extinction.

It is important to highlight that the simulated method must factor in the initial inception position of the mutant. This requires us to find all fixation probabilities arising from the inception of a mutant in any unique node. We then will average these probabilities over all of these inception positions to get what we mean by $\rho(G, C, r, \sigma)$, or the average fixation probability only based on the graph structure, coloring, and fitnesses.

Chapter 3

Results

Section 3.1

Network Connectedness

As discussed in literature, population or graph structure is one of the primary factors of interest that can affect fixation probability. Based on the two-clique and clique-like graphs we defined, we explore the resulting impact of the relationships within and between these islands on the success of a mutant type. We first simply look at how the two-clique model varies compared to a complete graph with no fitness heterogeneity of the same size, representing a homogeneous or well-mixed population. It is observed in Figure 3.1 that the singly-connected two-clique graph with green (light) and red (dark) nodes amplifies selection, while the n-connected and completely-connected two-clique graphs suppress selection. This highlights that island connectivity can greatly affect mutant survival.

We perform a robustness check for the fixation probability results for the singly-connected, n-connected, and completely-connected two-clique graphs with simulated calculations. In Appendix Figure A.4.1, we find nearly identical results.

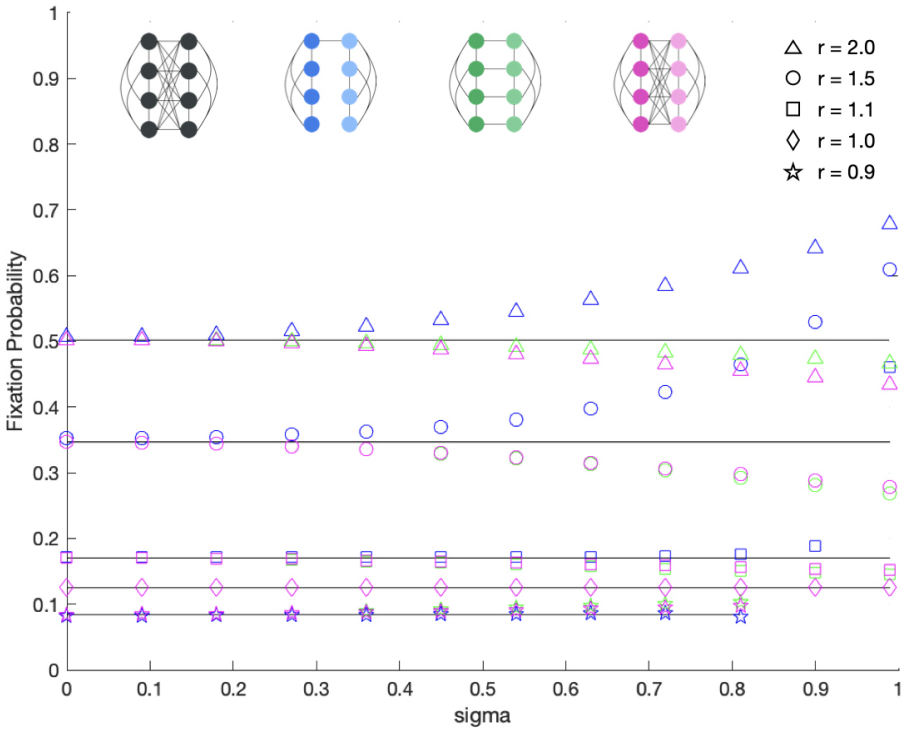

Figure 3.1: Fixation Probability on Well-Mixed and Two-Clique Models

This figure compares the singly-connected, n-connected, and completely-connected two-clique graphs of 8 nodes, to the complete, or well-mixed population across the various r values of 0.9, 1.0, 1.1, 1.5, and 2.0 and σ values from 0 to 0.99 (0.81 for $r = 0.9$). The black line corresponds to the well-mixed result, while the blue, green, and pink points correspond to the singly-connected, n-connected, and completely-connected two-clique graphs respectively. From the figure, we can see that for nearly all σ values, the singly-connected two-clique graph allows mutants to succeed with higher probabilities, while the n-connected and completely-connected graphs perform worse for mutants than the well-mixed complete graph.

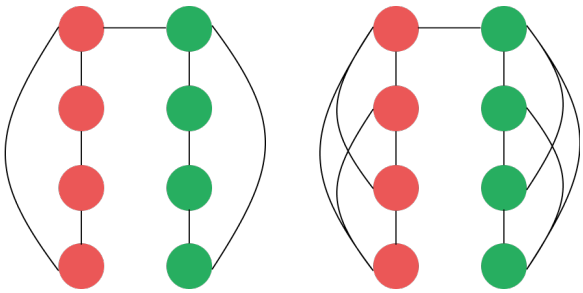

Figure 3.2: Varying Intra-connectedness

The graph on the left is a two-clique-like graph and the graph on the right is a two-clique graph. Due to the nature of these defined graphs, the two-clique graph is more intra-connected than the two-clique-like graph, as the former has completely-connected islands, while the latter only has cyclically-connected islands.

3.1.1. Intra-connectedness

We define intra-connectedness as the relationship among nodes of similar type within an island. To increase intra-connectedness means that one increases the number of adjacencies or connections inside of an island. We provide an example of changing intra-connectedness in Figure 3.2.

Hence, we explore how fixation probability differs for two-clique-like graphs and two-clique graphs, holding other factors constant for comparison purposes. Our results can be seen in Figure 3.3. We see that increasing the connectivity of the islands from clique-like subgraphs to clique subgraphs only modestly affects fixation probability. This is reasonable, given that a four-node cycle and complete graph differ by only two edges.

Based on Figure 3.3, in the singly-connected and n-connected cases, fixation probability for two-clique graphs surpasses that for two-clique-like graphs, but this flips once there is complete connectivity *between* cliques. Interestingly, fixation probability increases with σ for the singly-connected case across both two-clique and clique-like graphs but decreases with σ for the n-connected and completely-connected cases. We conclude that intra-connectivity alone cannot determine how likely it is for a mutant

to succeed, and that between island connectivity can affect fixation.

3.1.2. Inter-connectedness

Aside from within-island relationships, we evaluate the evolutionary benefit of having more connections between dissimilar node types. We define inter-connectedness as the relationship among nodes of different types between two islands, like a bipartite relationship. We provide an examples of increases in these inter-connections in Figure 3.4. Let us define the types of increases as follows: a) represents a *star-like* increase in connectivity, b) represents a *linear* increase in connectivity, and c) represents a *zig-zag* increase in connectivity. We can see that this star-like increase in connectivity is asymmetric, and increases the degree of one node for one type and all nodes for the other type. Increasing connectivity linearly eventually increases the degrees of all nodes of both types by one, and increasing connectivity in the zig-zag manner increases the degrees of by about one until completely connectivity is reached between the islands.

One could hypothesize that increasing the inter-connectivity of a graph could increase a mutant's ability to dominate the graph, given a constant fitness, as the mutant's offspring will have access to more nodes. For the linear increase in inter-connectedness, we see in Figure 3.5 that as fitness fluctuations increase in both red and green nodes, increasing the number of connections between the red and green nodes (here displayed as dark and light nodes respectively) *decreases* the mutant's likelihood of fixation for $r > 1$ and increases it for $r < 1$. In other words, increasing linear inter-connectedness suppresses selection. We observe this pattern in a two-clique-like graph with eight nodes and larger size graph of $N = 10$ as well (Appendix Figures A.4.2 and A.4.3). This may be a result of increasing inter-connectivity causing the graphs to diverge from being star-like structures with one or two central nodes, as in the singly-connected case.

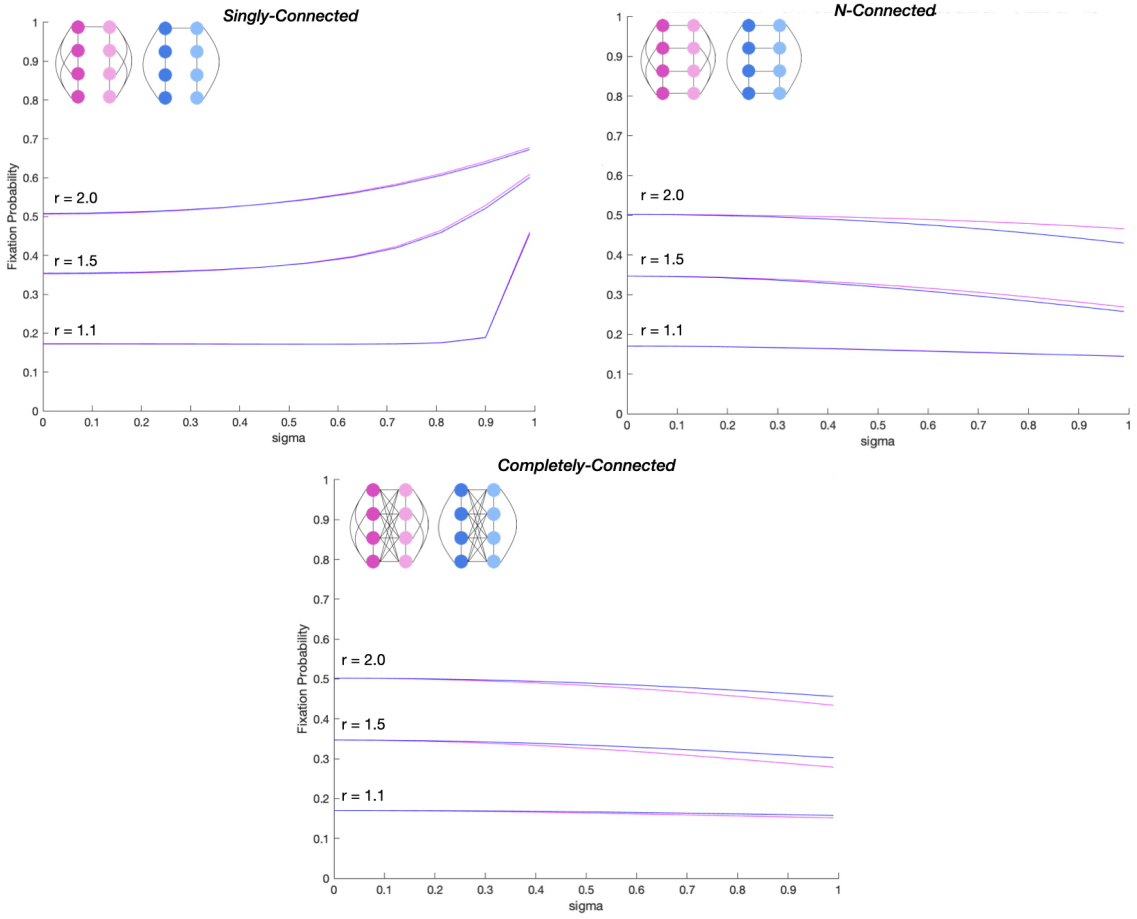

Figure 3.3: Fixation Probability Given Increasing Intra-connectedness

This figure compares the singly-connected, n-connected, and completely-connected two-clique graphs of 8 nodes to the singly-connected, n-connected, and completely-connected two-clique-like graphs of 8 nodes across the various r values of 1.1, 1.5, and 2.0 and σ values from 0 to 0.99. The top-left panel compares the singly-connected graphs, the top-right compares the n-connected graphs, and the bottom-middle compares the completely-connected graphs. The pink lines represent two-clique graphs while the blue lines represent two-clique-like graphs.

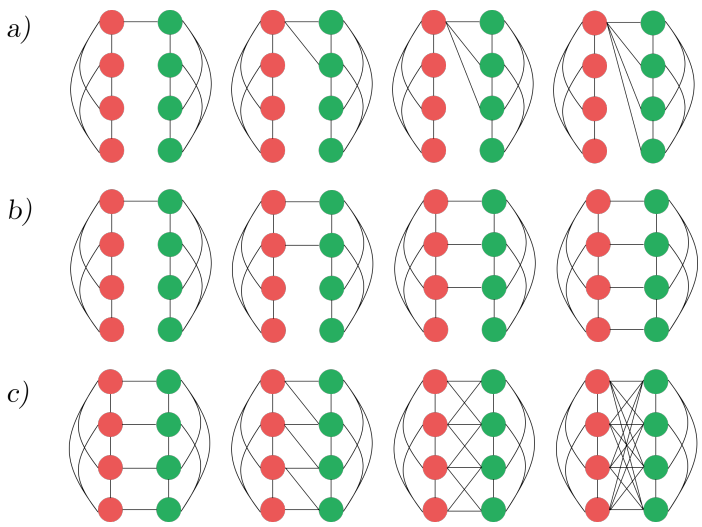

Figure 3.4: Varying Inter-connectedness

For parts a), b), and c), inter-connectedness increases as we move from left to right, as more nodes are adjacent to nodes of the opposite type. We note that a) provides asymmetry between the islands, while b) and c) maintain that the two islands have the same number of nodes with the exact same degrees. Also, we call attention to the fact that these inter-connections can be repeated for two-clique-like graphs with cyclic islands.

We also evaluate how increasing inter-connectivity in the zig-zag fashion affects fixation probability. As shown in Figure 3.6, increasing inter-connectivity by increasing the degree of all of the nodes dose not produce as stark of a difference in fixation probability that linear increases caused. While the two-clique-like result, in Appendix Figure A.4.4, reveals that more inter-connectivity could translate to a lower decrease in fixation likelihood as σ increases, this difference is slight, so the results for two-clique and clique-like graphs are similar. This suggests that perhaps once each node on an island is sufficiently connected to the other island, increases in inter-connectivity do not largely impact fixation. However, we also note that once every node in an island is at least connected to one node in the other island, the graph structure is a suppressor of selection.

We lastly consider the asymmetric case of increasing inter-connectedness. Figure

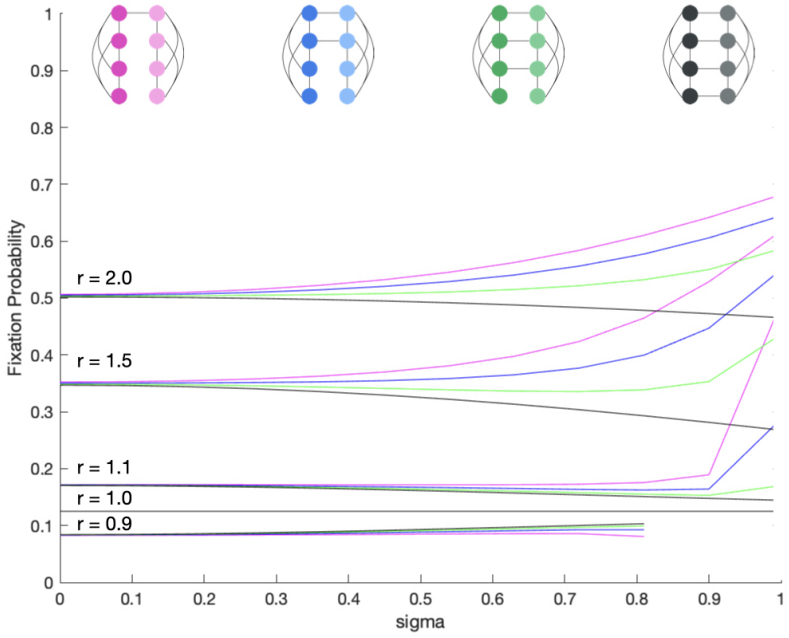

Figure 3.5: Linear Increasing of Inter-Connectedness in Two-Clique Graphs

This figure compares the singly-connected, doubly-connected, triply-connected, and n-connected two-clique graphs of 8 nodes across the various r values of 0.9, 1.0, 1.1, 1.5, and 2.0 and σ values from 0 to 0.99 (0.81 for $r = 0.81$). The pink, blue, green, and black lines represent the singly-connected, doubly-connected, triply-connected, and n-connected graphs respectively.

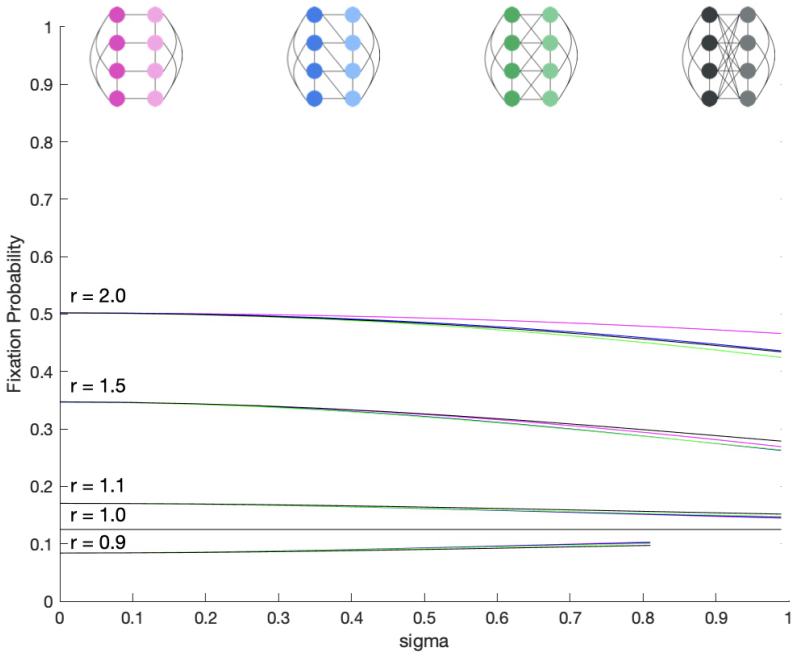

Figure 3.6: Zig-Zag Increasing of Inter-Connectedness in Two-Clique Graphs

This figure compares the n-connected, zig-zag-connected, cross-connected, and completely-connected two-clique graphs of 8 nodes across the various r values of 0.9, 1.0, 1.1, 1.5, and 2.0 and σ values from 0 to 0.99 (0.81 for $r = 0.81$). The pink, blue, green, and black lines represent the n-connected, zig-zag-connected, cross-connected, and completely-connected graphs respectively.

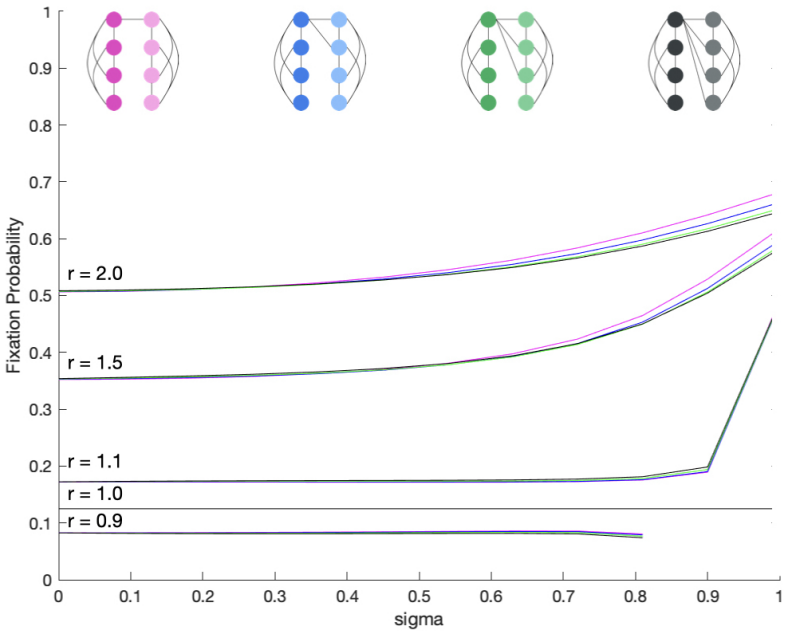

Figure 3.7: Star-Like Increasing of Inter-Connectedness in Two-Cliques

This figure compares graphs with one, two, three, and four star-like inter-connected two-clique graphs of 8 nodes across the various r values of 0.9, 1.0, 1.1, 1.5, and 2.0 and σ values from 0 to 0.99 (0.81 for $r = 0.81$). The pink, blue, green, and black lines represent the graphs with one, two, three, and four star-like between-clique connections respectively.

3.7 and Appendix Figure A.4.5 confirms two patterns; firstly, the star-like nature of the inter-island connectivity results in these graph structures amplifying selection, and secondly, as not every node in each island is connected to the other island, we do not see a decrease in fixation probability as σ increases.

Section 3.2

Unbalalanced Graphs

One underlying assumption of the models we have thus considered is that the islands of different types are the same size. We loosen this assumption here to understand how varying the quantity of resource beneficial and detrimental nodes can affect mutants' survival. Figure 3.8 illustrates how changing the island size of the low resource quality

cyclic island impacts fixation probability. It can be seen that the greater number of nodes of the red type, the more of an amplifier of selection the graph is. This draws from previous conclusions that the star is a common amplifier, and the 1-7 two-clique graph is the most star-like. This finding follows the literature, as clique-stars, or stars with large central cliques, as defined by Choi and Yu (2018) amplify selection [12]. What is most interesting is that when the star-like structure has a majority of green nodes, the fixation probability decreases with greater σ values. This could result from the fact that in the case where more nodes are green, the *central* node of the star-like structure is red, which harms a mutant's ability (or any individual's ability) to fixate in that node. We see similar behaviors in two-clique-like graphs, as shown in Appendix Figure A.4.6.

Figures 3.9 and 3.10 displays how inter-connectivity interacts with changing islands sizes. We see that the more inter-connected the islands are, the less successful the mutant is given larger environmental variation which is consistent with balanced two-clique graphs.

Section 3.3

Varying Fitness Heterogeneity

While all previous results in this paper have focused on the assumption of background fitness heterogeneity, where $\sigma_a = \sigma_b$, we transition to looking at other fitness models. As mentioned in literature, mutants and residents can have exactly opposite fitness deviations ($\sigma_a = -\sigma_b$), or one of the types can have no deviation ($\sigma_a = 0$ or $\sigma_b = 0$). We explore these assumptions and evaluate how they change our results. We can initially explore these results in Figure 3.11, where we can see that all models perform relatively similarly, but also that background, opposite, and mutant fitness heterogeneity may see lower fixation at higher σ values. We explore each model more

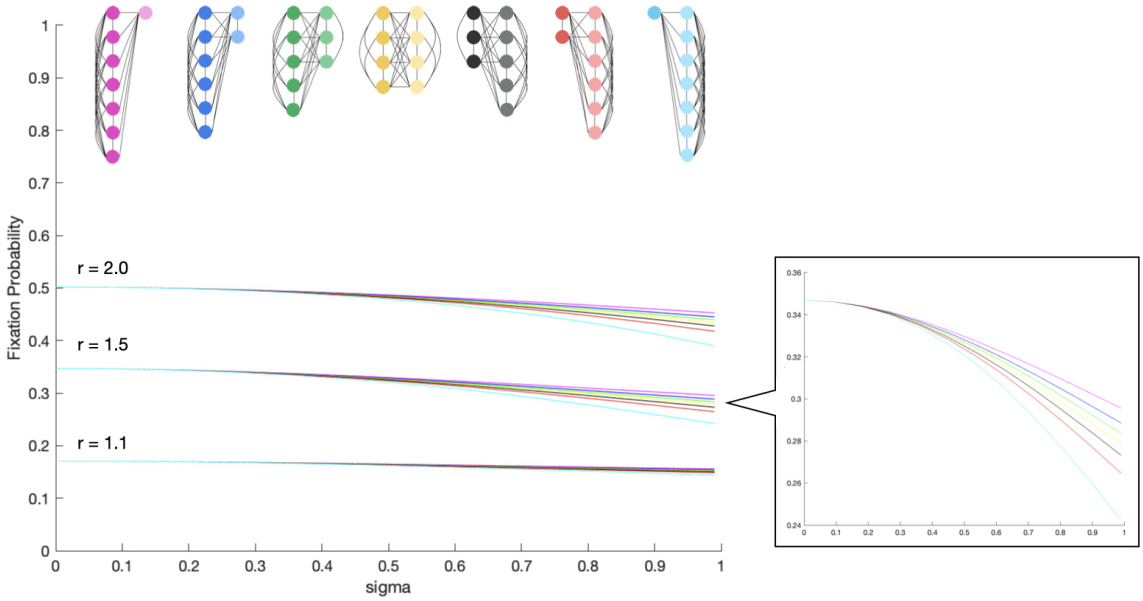

Figure 3.8: Varying Island Sizes of Two-Clique Graphs

This figure displays fixation probability for seven different graphs, six of which have unbalanced island sizes across σ value of 0 to 0.99 for r values 1.1, 1.5, and 2.0. Each line color corresponds to the colored graph displayed above. We note that in the calculation of these fixation probabilities, we keep the standard deviation of fitness constant at σ. However, because the number of green and red nodes changes across graph structures, to hold constant the overall standard deviation across graphs, we adjust the resulting deviation in red and green nodes for each graph as follows. For 1-7 or 7-1 structures, the single node has deviations of +/- $\sqrt{7} \cdot \sigma$, while the other seven nodes have deviations of +/- $\frac{\sqrt{7}}{7} \cdot \sigma$. For 2-6 or 6-2 structures, the isolated pair of nodes have deviations of +/- $\sqrt{3} \cdot \sigma$, while the other six nodes have deviations of +/- $\frac{\sqrt{3}}{3} \cdot \sigma$. Lastly, for 3-5 or 5-3 structures, the three nodes have deviations of +/- $\frac{\sqrt{15}}{3} \cdot \sigma$, while the other five nodes have deviations of +/- $\frac{\sqrt{15}}{5} \cdot \sigma$.

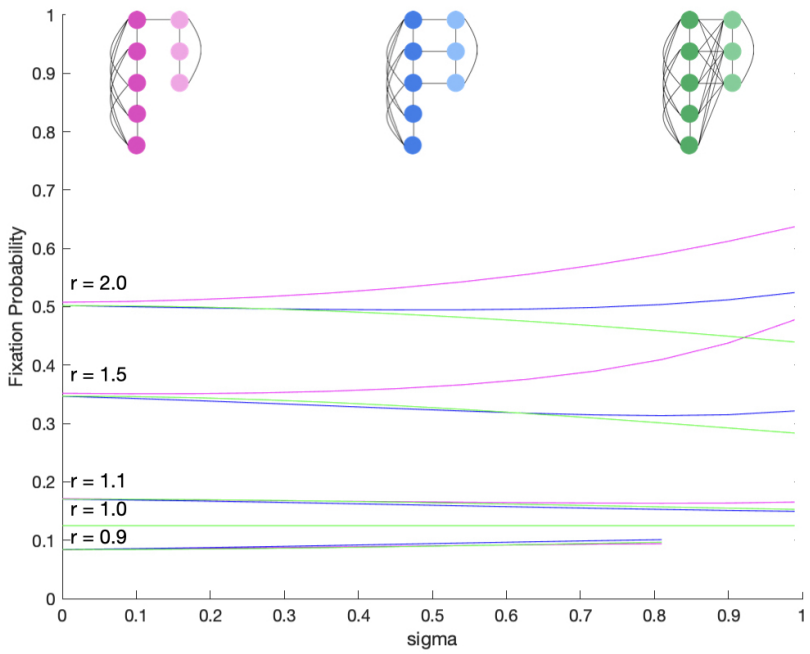

Figure 3.9: Unbalanced 3-5 Two-Clique Graph

This figure compares the singly-connected, n-connected, completely-connected unbalanced two-clique graphs with five red nodes and three green nodes. These comparisons are across the various r values of 0.9, 1.0, 1.1, 1.5, and 2.0 and σ values from 0 to 0.99 (0.81 for $r = 0.81$). The pink, blue, green, and black lines correspond to the singly-connected, n-connected, completely-connected graphs respectively.

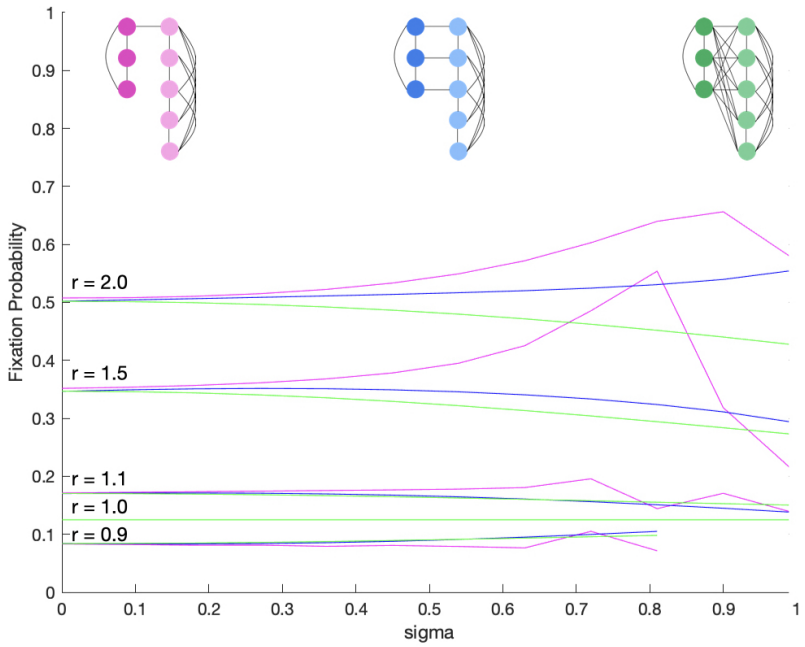

Figure 3.10: Unbalanced 5-3 Two-Clique Graph

This figure compares the singly-connected, n-connected, completely-connected unbalanced two-clique graphs with three red nodes and five green nodes. These comparisons are across the various r values of 0.9, 1.0, 1.1, 1.5, and 2.0 and σ values from 0 to 0.99 (0.81 for $r = 0.81$). The pink, blue, green, and black lines correspond to the singly-connected, n-connected, completely-connected graphs respectively. We can see that for particular values of σ, specifically around 0.81, fixation probability peaks for the singly-connected graph for larger r values. This could translate to fitness deviations providing conditions that are extremely favorable for the advantageous mutant compared to the resident, unlike larger σ values that could negatively impact mutant success.

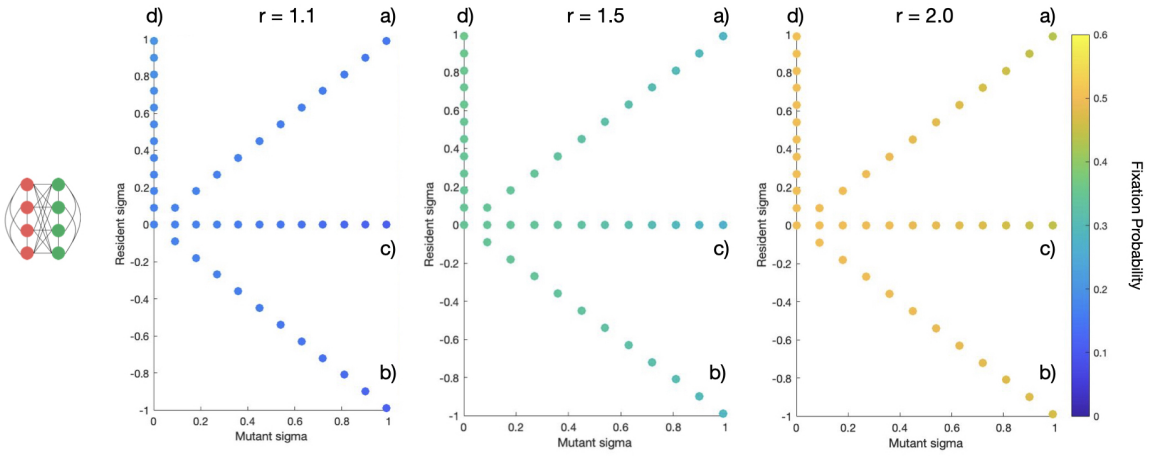

Figure 3.11: Fixation Probability of Completely-Connected Two-Clique Graph with Opposite, Mutant, and Resident Heterogeneity

This figure displays at fixation probability in terms of σ_a, the mutant's sigma, and σ_b, the resident's sigma, for the completely-connected two-clique 8 node graph. Each of the three panels compares background, opposite, mutant, and resident heterogeneity across σ values of 0 to 0.99 for the mutant and -0.99 to 0.99 for the resident. The left panel shows fixation probability for $r = 1.1$, the middle panel shows fixation probability for $r = 1.5$, and the right panel shows fixation probability for $r = 2.0$. In this figure, a) refers to the background fitness heterogeneity model, where $\sigma_a = \sigma_b$, b) refers to opposite fitness heterogeneity, where $\sigma_a = -\sigma_b$, c) refers to mutant heterogeneity, where $\sigma_b = 0$, and d) refers to resident heterogeneity, where $\sigma_a = 0$.

in depth in the figures below.

3.3.1. Opposite Heterogeneity

We first consider opposite heterogeneity, where nodes that are beneficial for the mutant type are detrimental to the resident type and vice versa. Figure 3.12 reveals that one major impact of this opposite heterogeneity is on the n-connected graph structure, whose fixation probability now exceeds that of the complete, well-mixed population for all r and σ values. Interestingly, we also find that background fitness heterogeneity only wins in cases of larger mutant advantage (higher r values) in the singly-connected two-clique model.

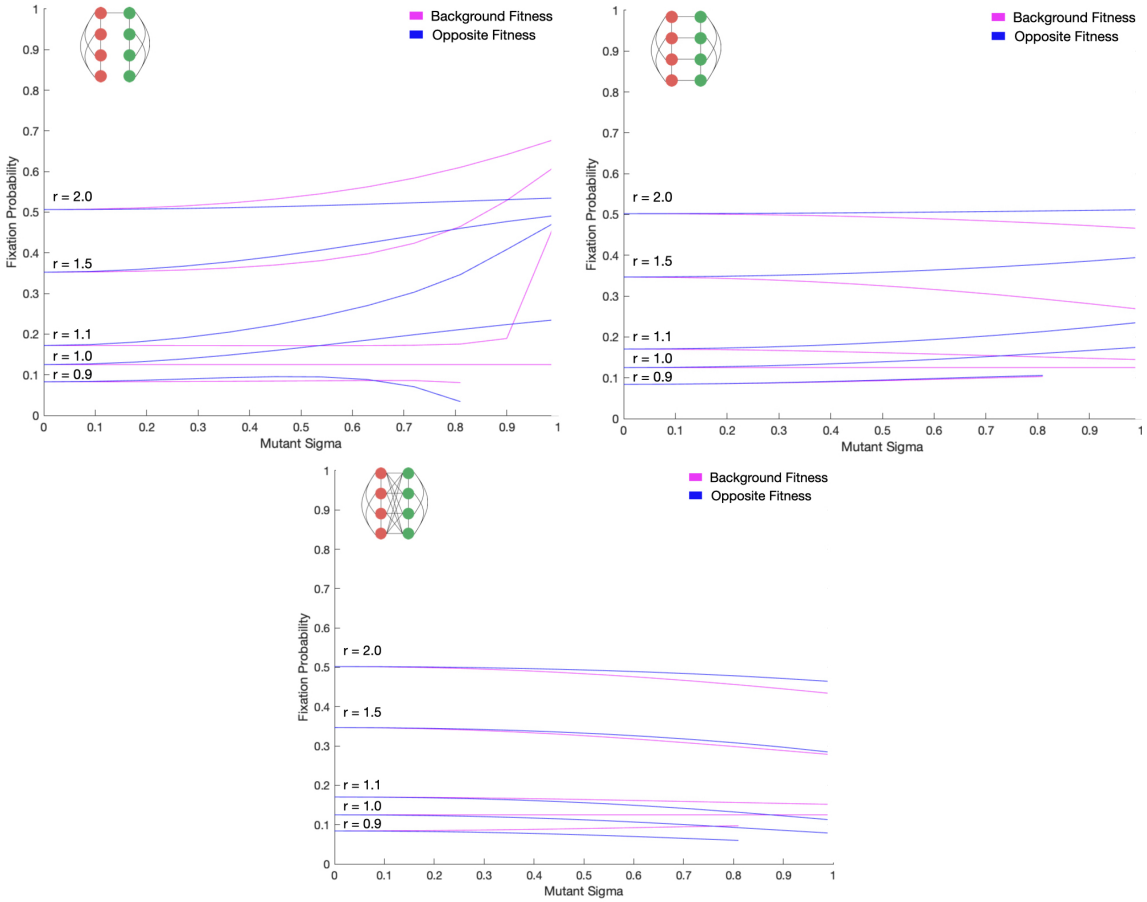

Figure 3.12: Fixation Probability of Completely-Connected Two-Clique Graph with Background vs Opposite Fitness Heterogeneity

Each of the three figures compares background fitness heterogeneity (pink lines) to opposite fitness heterogeneity (blue lines), across r values of 0.9, 1.0, 1.1, 1.5 and 2.0, and σ_a values from 0 to 0.99 (0.81 for $r = 0.9$). The top-left panel looks at the singly-connected two-clique 8 node graph, the top-right panel looks at the n-connected two-clique 8 node graph, and the bottom-middle panel looks at the completely-connected two-clique 8 node graph.

3.3.2. Mutant Heterogeneity

Next, we look at mutant heterogeneity, where only the mutant experiences resource heterogeneity or environmental variation. Figure 3.13 reveals, in contrast to opposite heterogeneity, that mutant heterogeneity does not amplify fixation with the n-connected two-clique graph. Interestingly, we see that of the three other models, background fitness heterogeneity finds most similarity with the mutant heterogeneity model for the n-connected and completely-connected graphs, which follows because we are primarily observing how mutants perform in response to their environment with fixation probability.

3.3.3. Resident Heterogeneity

Lastly, we observe resident heterogeneity, where only the resident experiences resource heterogeneity or environmental variation. Figure 3.14 reveals once again that resident heterogeneity amplifies fixation with the n-connected two-clique graph. When observing all four models, it seems as though the resident heterogeneity model allows the mutant to perform most successfully across the three types of graphs considered in almost all specifications. This suggests that environmental variation hurts mutants, even when some of this variation is beneficial. This is supported by the fact that with resident heterogeneity, the resident can achieve a fitness that is at most or slightly higher than the mutant, while in contrast to the mutant, the resident also suffers from detrimental variation as well.

Section 3.4

Dynamic Coloring

Dynamic coloring involves the active changing of environmental characteristics of nodes that contribute to fitnesses. On bipartite graphs, Kaveh et al. find that in-

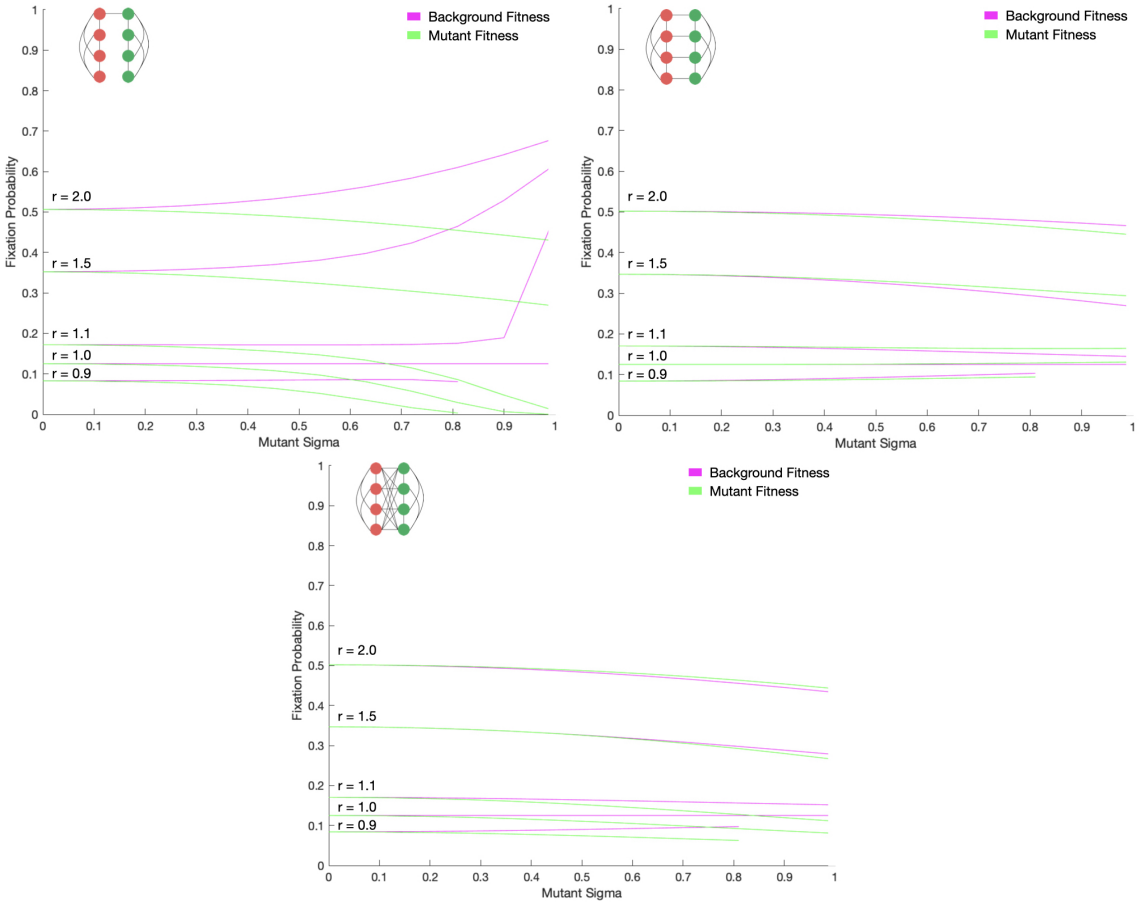

Figure 3.13: Fixation Probability of Completely-Connected Two-Clique Graph with Background vs Mutant Fitness Heterogeneity

Each of the three figures compares background fitness heterogeneity (pink lines) to mutant fitness heterogeneity (green lines), across r values of 0.9, 1.0, 1.1, 1.5 and 2.0, and σ_a values from 0 to 0.99 (0.81 for $r = 0.9$). The top-left panel looks at the singly-connected two-clique 8 node graph, the top-right panel looks at the n-connected two-clique 8 node graph, and the bottom-middle panel looks at the completely-connected two-clique 8 node graph.

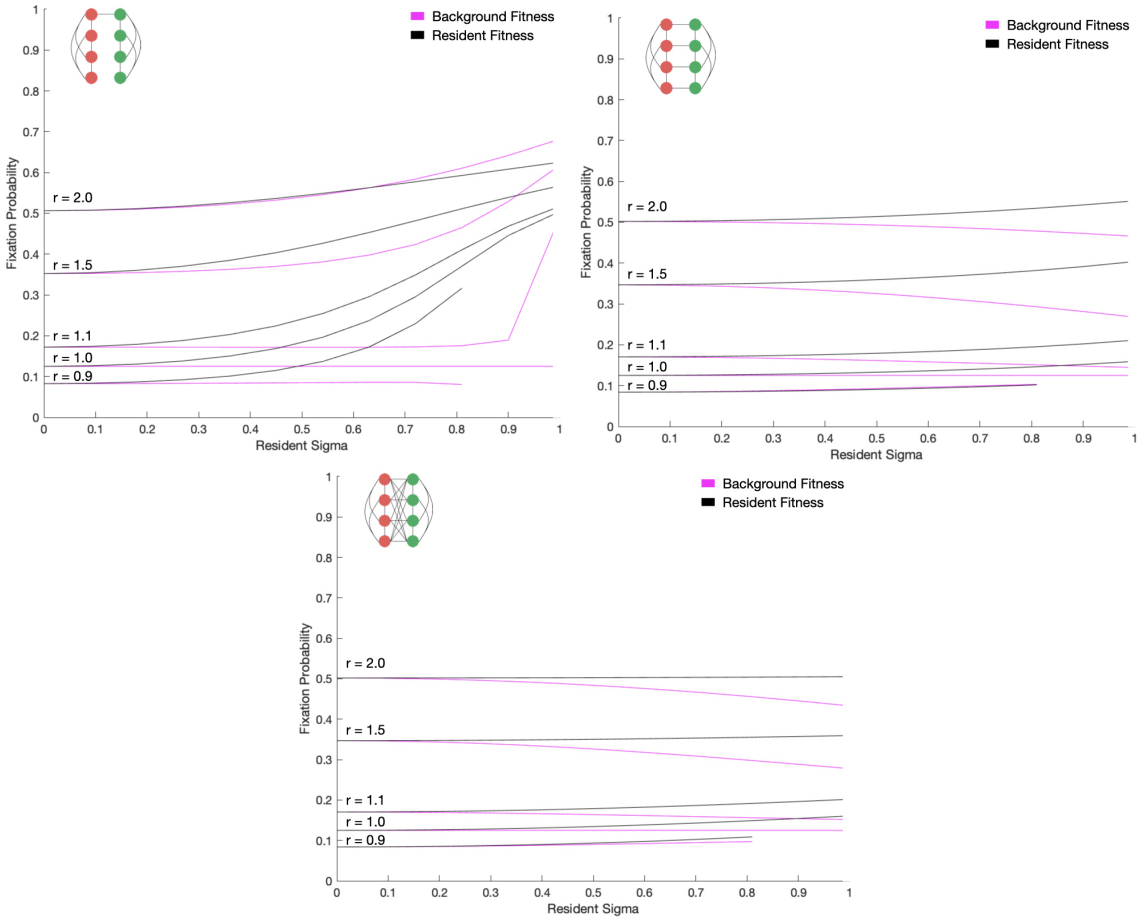

Figure 3.14: Fixation Probability of Completely-Connected Two-Clique Graph with Background vs Resident Fitness Heterogeneity

Each of the three figures compares background fitness heterogeneity (pink lines) to resident fitness heterogeneity (black lines), across r values of 0.9, 1.0, 1.1, 1.5 and 2.0, and σ_b values from 0 to 0.99 (0.81 for $r = 0.9$). The top-left panel looks at the singly-connected two-clique 8 node graph, the top-right panel looks at the n-connected two-clique 8 node graph, and the bottom-middle panel looks at the completely-connected two-clique 8 node graph.

creasing the movement of resource quality around a network increases the effects of strong heterogeneity and decreases the effects of weaker heterogeneity on fixation probability [16]. We explore the impact of dynamic coloring on the two-clique and two-clique-like graphs we consider in this paper.

First, we describe our process. Exploring dynamic coloring necessitates a simulation-based approach in order to randomly assign environmental quality to nodes at each time step. We model a beneficial environment that randomly can deteriorate over time. To do this, we suppose that green, or beneficial, nodes will become red, or detrimental, nodes until a certain proportion of green nodes have switched. This attempts to model high-quality resource depletion. However, once enough of these green nodes have converted to red nodes, we allow them to revert back to being high-quality green nodes, suggesting the environment was able to replenish its resources. We augment the method from Model and Methods 2.3 Simulation Approach to illustrate these assumptions. After picking a random node to be replaced at each time step, we add:

- Given a probability p and a maximum proportion of possible green node to red node conversions m, if m has not been attained, choose a random green node to become a red node with probability p. If m has been met, then choose one of the converted red nodes to become a green node once again.

An example of the coloring changes that occurs to a graph during this dynamic simulation can be found in Figure 3.15.

The results of performing this dynamic coloring on the graphs of interest from Figure 2.2 can be seen in Figure 3.16 (and Figure A.4.7 in the Appendix). As seen by the difference between the solid (representing dynamic coloring) and dashed (representing static coloring) lines, for nearly all mutant inception points and graph structure specifications, dynamic coloring increases a mutant's likelihood of fixating given in-

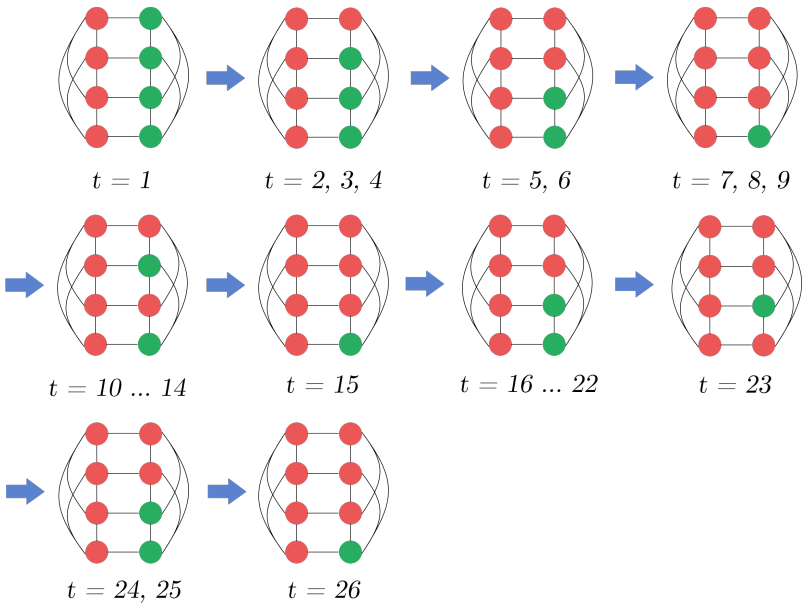

Figure 3.15: Example of Simulated Dynamic Coloring on N-Connected Two-Clique Graph

This figure is just one example of dynamic coloring on a graph with a 0.25 recoloring probability p and a maximum green to red conversation threshold, m, of 0.75, when $r = 1.5$ and $\sigma = 0.5$. We can see that all green nodes do not convert to red, due to the imposed threshold, and that once this threshold is reached, some nodes can be replenished and can revert to green.

creasing environmental variability. This suggests that mutant resilience is amplified further when resource depletion occurs; mutant types are less harmed by environments with low quality resources than resident types are. This model also finds that the n-connected two-clique graph, previously a suppressor of selection in the static coloring environment, amplifies selection in a dynamic one. While there are many other dynamic coloring models, we find here that resource degradation might not harm, and may even help, the chances of mutant fixation.

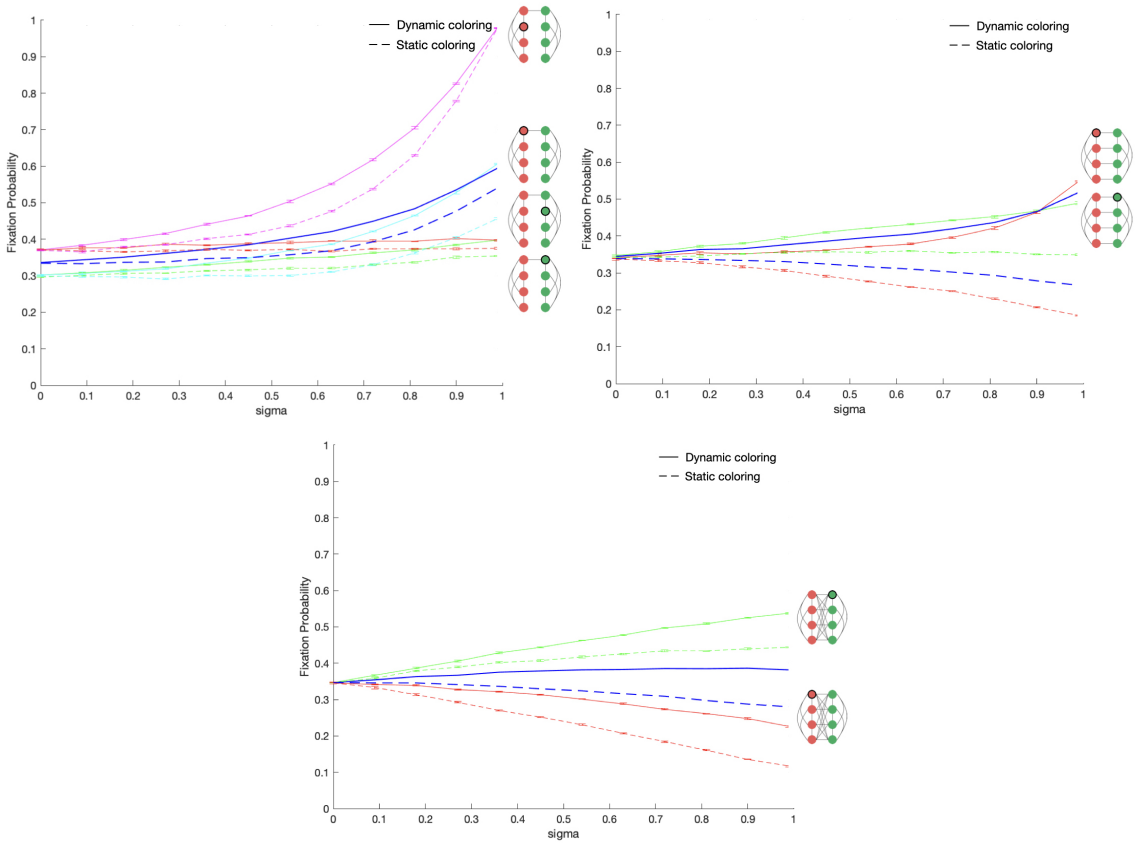

Figure 3.16: Fixation Probability of Singly-Connected, N-Connected, Completely-Connected Two-Clique Graph with Dynamic and Static Coloring

This figure displays the results of dynamic coloring on two-clique graphs, with $p = 0.25$, $m = 0.75$, and $r = 1.5$ across σ values from 0 to 0.99. The top-left panel corresponds to the singly-connected graph, the top-right panel corresponds to the n-connected graph, and the bottom-middle panel corresponds to the completely-connected graph. In all figures, the bolded blue solid and dashed lines represent the average fixation probabilities, while the various other colors represent different mutant initialization nodes, captured by the graph diagrams on the right.

Chapter 4

Discussion

Our results explore the impacts of varying population structures and environmental characteristics of nodes on mutant fixation probability. Through four different analyses, we find that mutants succeed in environments of decreased inter-connectivity, decreased high-quality resources, and decreased environmental variability.

Section 4.1

Analysis

We first evaluate how network connectivity between and within cliques and clique-like subgraphs can influence fixation probability. We find that two-clique graphs can be both amplifiers and suppressors of selection, depending on these connections between cliques and clique-like groups. The difference between two-clique and clique-like graphs is seemingly negligible, as they perform similarly. However, once inter-connectivity is introduced, larger changes in mutant success can arise. We observe that increasing inter-connectivity in a balanced way, distributed evenly and symmetrically across nodes (linear increasing of inter-connectivity) influences fixation probability more than when increasing connections between cliques in a zig-zag or star-like fashion. Overall, while increasing the intra-connectivity of subgraphs can

influence (both increase and decrease) fixation probabilities as environmental variability increases, inter-connectivity plays a much larger role in fixation probability. We conclude that the more linear inter-connectivity between cliques, the less likely the mutant is to succeed as environmental variability increases.

Another aspect of population structure we evaluate is how fixation changes when island size changes. We find that while the relative size of cliques does not influence fixation probability much, when larger cliques are composed of red nodes, the fixation probability is higher, and this increases as red node clique sizes increase. Hence, thee larger the share of low-quality resource nodes, the higher the fixation probability as environmental variability increases. Additionally, the trend of increasing inter-connectivity leading to lower fixation probability generally holds for unbalanced graphs as well.

We move on to our exploration of environmental differences across the nodes in our graphs. In our evaluation of four fitness heterogeneity models, we find that typically, given higher inter-connectivity among cliques, other fitness models perform similarly, if not better, than background fitness heterogeneity. In fact, only in the singly-connected two-clique case do identical environmental deviations for mutants and residents (background fitness heterogeneity) help advantageous mutants (those with a higher r) fixate. We also observe that the resident fitness heterogeneity model seems to result in the highest fixation probability for our structures of interest, revealing that mutants have the most opportunity for success when they are not subject to fluctuations in their fitness.

Lastly, we study dynamic coloring, and find that in almost all cases, resource depletion and introducing dynamic coloring increases fixation probability. These effect sizes vary by graph type; the n-connected two-clique, which typically suppresses selection, amplifies selection at $r = 1.5$ with dynamic coloring. We conclude that

resource depletion (and a periodic replenishment if applicable) increases a mutant's likelihood of success across two-clique graph inter-connectivity, inception nodes, and environmental variability.

4.1.1. Implications

This work, while based on simplified models, provide insights into a variety of real-world instances. From biological phenomena like cell growth and reproduction, to ecological processes including species migration, to social phenomena such as human interaction, populations and individuals within populations face certain dynamics and relationships that can modeled. Any underlying trends we have found as a result of varying assumptions in these models can be applied to actual scenarios, allowing our work to actively take part in our discovery of how the world works.

Section 4.2

Future Research

One main aspect of this paper includes small graphs of eight to ten nodes. While these simplified models provide insights on small-scale evolutionary dynamics, these models can be the building motifs for larger graphs. Our methods could be extended for larger graphs to allow us to verify if the results we find are maintained across population and clique size.

Other dimensions of exploration involve expanding from two cliques and two colors to multi-clique and multi-colored graphs. While less variability in our models through binary differences in colors and islands provides simplicity, the real world is riddled with a spectrum of variability, and modeling this could provide further insights.

An additional area with more potential for exploration is the study of dynamic coloring and environmental variation. In this paper, we explore the cyclic depletion

and revival of high quality resource locations. However, many other types of environmental fluctuations could exist in reality and in a model, including cyclic weather or climate changes, the physical movement of resources between nodes, random assignment of environmental quality each year, and even the colonization of one type of environmental resource by another. It would be interesting to further pursue how these assumptions and model characteristics could influence the dynamics between the types interacting with these environments.

Section 4.3

Conclusion

The field of modeling evolutionary dynamics is constantly expanding, with plenty of promising future work to continue probing how various factors influence the success of different types. We explore four alternate specifications of the Moran process on a particular graph to identify how graph structure and graph coloring influence fixation probability. Our results reveal a trend that the mutant typically prefers the lesser of two evils–for example, resource depletion is beneficial for the mutant, especially because the resident type has to experience it as well! Future exploration can continue to push the boundaries of what we know of evolutionary dynamics, identifying and verifying conditions in mutant behavior in the fight for survival.

Bibliography

[1] Benjamin Allen and Martin A. Nowak, *Games on graphs*, EMS Surveys in Mathematical Sciences (2014), 113–151.

[2] N. H. Barton, *The probability of fixation of a favoured allele in a subdivided population*, Genetic Research **62** (1993), no. 2, 149–157.

[3] Martin A. Nowak Christine Taylor, Yoh Iwasa.

[4] Martin A. Nowak Erez Lieberman, Christoph Hauert, *Evolutionary dynamics on graphs*, Nature **433** (2005), 312–316.

[5] Eliza M. Ferreira Armando G. M. Neves Evandro P. de Souza, *Fixation probabilities for the moran process in evolutionary games with two strategies: graph shapes and large population asymptotics*, Journal of Mathematical Biology **78** (2019), 1033–1065.

[6] Á.Lozano Rojo F.Alcalde Cuesta, P.González Sequeiros, *Fast and asymptotic computation of the fixation probability for moran processes on graphs*, Biosystems **129** (2015), 25–35.

[7] Patrick Fitzpatrick, *Local moran process on graphs*, Center for Theoretical Physics (2018).

[8] Joel H. Spencer Fred S. Roberts, *A characterization of clique graphs*, Journal of Combinatorial Theory **10** (1971), 102–108.

[9] Laura Hindersin and Arne Traulsen, *Counterintuitive properties of the fixation time in network-structured populations*, Journal of the Royal Society Interface **11** (2014), no. 20140606.

[10] Laura Hindsersin, *Fixation times in graph-structured populations.*

[11] Kamran Kaveh Hossein Nemati, Mohammad Reza Ejtehadi, *Counterintuitive properties of fixation probability and fixation time in population structures with spatially periodic resource distribution*, arXiv (2022).

[12] Unjong Yu Jeong-Ok Choi, *Fixation probability on clique-based graphs*, Physica A: Statistical Mechanics and its Applications **492** (2018), 2129–2135.

[13] Krishnendu Chatterjee Josef Tkadlec, Andreas Pavlogiannis and Martin A. Nowak, *Population structure determines the tradeoff between fixation probability and fixation time*, Communications Biology **2** (2019), no. 138.

[14] Krishnendu Chatterjee Martin A. Nowak Josef Tkadlec, Andreas Pavlogiannis, *Population structure determines the tradeoff between fixation probability and fixation time*, Communications Biology **2** (2019), no. 138.

[15] George B. Mertzios David Richerby Maria Serna Josep Díaz, Leslie Ann Goldberg and Paul G. Spirakisr, *On the fixation probability of superstars*, Proceedings of the Royal Society **469** (2013), no. 2156.

[16] Krishnendu Chatterjee Martin A. Nowak Kamran Kaveh, Alex McAvoy, *The moran process on 2-chromatic graphs*, PLoS Computational Biology **16** (2020), no. 11.

[17] Motoo Kimura, *On the probability of fixation of mutant genes in a population*, Genetics **47** (1962), no. 6, 713–719.

[18] Rasmus Ibsen-Jensen Krishnendu Chatterjee and Martin A. Nowak, *Faster monte-carlo algorithms for fixation probability of the moran process on undirected graphs*, (2022).

[19] J. Rychtář M. Broom and B. Stadler, *Evolutionary dynamics on small-order graphs*, Journal of Interdisciplinary Mathematics **12** (2009), no. 2, 129–140.

[20] J. Rychtář B. T. Stadler M. Broom, *Evolutionary dynamics on graphs - the effect of graph structure and initial placement on mutant spread*, Journal of Statistical Theory and Practice **5** (2011), no. 3, 369–381.

[21] Alex McAvoy Madison S. Krieger and Martin A. Nowak, *Effects of motion in structured populations*, Journal of the Royal Society Interface **14** (2017), no. 135.

[22] Arne Traulsen Marius Möller, Laura Hindersin, *Exploring and mapping the universe of evolutionary graphs identifies structural properties affecting fixation probability and time*, Communications Biology **2** (2019), no. 137.

[23] Naoki Masuda, *Voter model on the two-clique graph*, (2018).

[24] Amir Hossein Darooneh Mohammad Ali Dehghani and Mohammad Kohandel, *The network structure affects the fixation probability when it couples to the birth-death dynamics in finite population*, PLos Computational Biology (2021).

[25] Martin A. Nowak, *Evolutionary dynamics: exploring the equations of life*, Belknap Press of Harvard University Press, Cambridge, Massachusetts, 2006.

[26] Arne Traulsen Peter Czuppon, *Understanding evolutionary and ecological dynamics using a continuum limit*, Ecology and Evolution **11** (2021), no. 11, 5857–5873.

[27] Jan Rychtár and Dewey T. Taylor, *Moran process and wright-fisher process favor low variability*, Discrete and Continuous Dynamical Systems Series B **26** (2021), no. 7, 3491–3504.

[28] Montgomery Slatkin, *Fixation probabilities and fixation times in a subdivided population*, Evolution **35** (1981), no. 3, 477–488.

[29] Fabio A. C. C. Chalub Max O. Souza, *Fixation in large populations: a continuous view of a discrete problem*, Journal of Mathematical Biology **72** (2016), 283–330.

[30] Gregory J. Puleo Wes Maciejewski, *Environmental evolutionary graph theory*, Journal of Theoretical Biology **360** (2014), 117–128.

Appendix

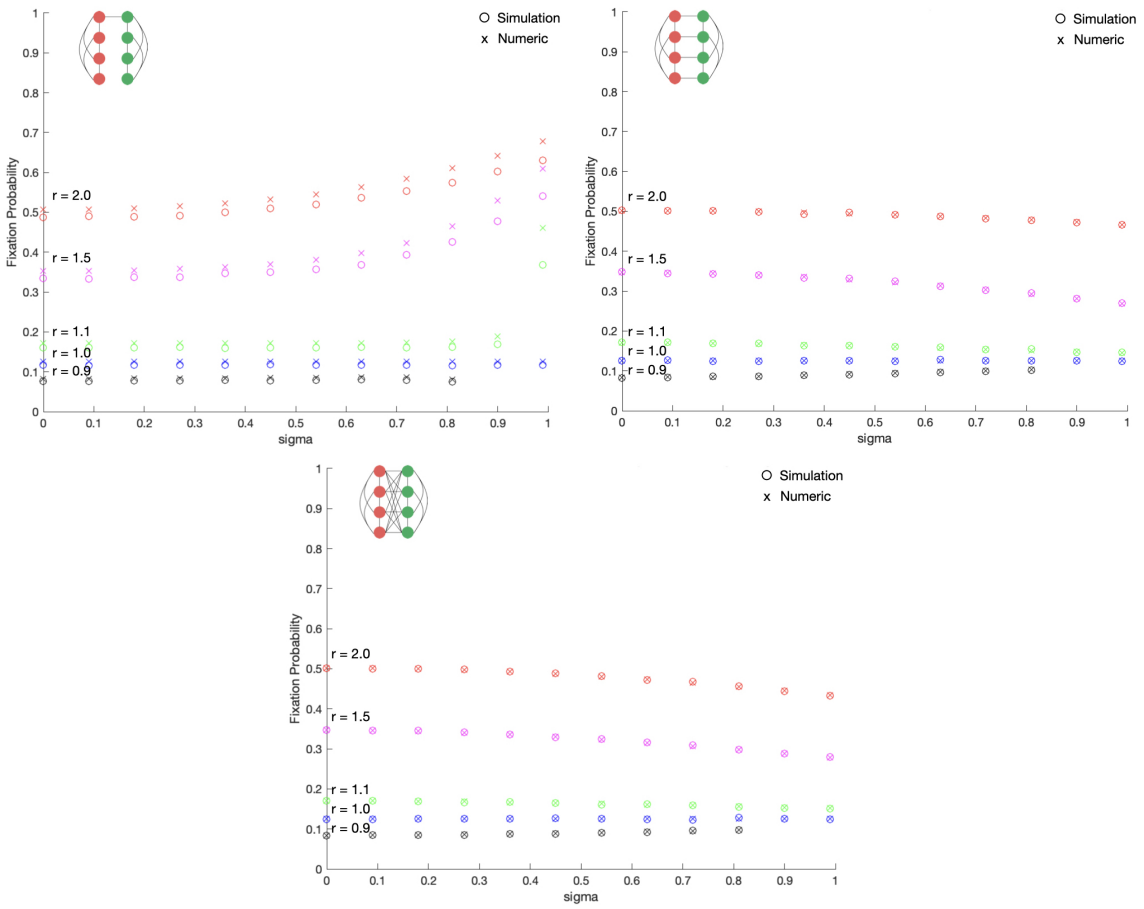

Figure A.4.1: Fixation Probability of Singly-Connected, N-Connected, Completely-Connected Two-Clique-Like Graph with Simulation and Numerically Solved Calculations

This figure displays the results of algebraic (shown by "x") and simulation (shown by "o") fixation probability on two-clique graphs across r values of 0.9, 1.0, 1.1, 1.5, and 2.0, and σ values from 0 to 0.99 (0.81 for $r = 0.9$). The colors represent different r values, where 0.9, 1.0, 1.1, 1.5, 2.0 are black, blue, green, pink, and red respectively. The top-left corresponds to the singly-connected two-clique 8 node graph, the top-right corresponds to the n-connected two-clique 8 node graph, and the bottom-middle corresponds to the completely-connected two-clique 8 node graph.

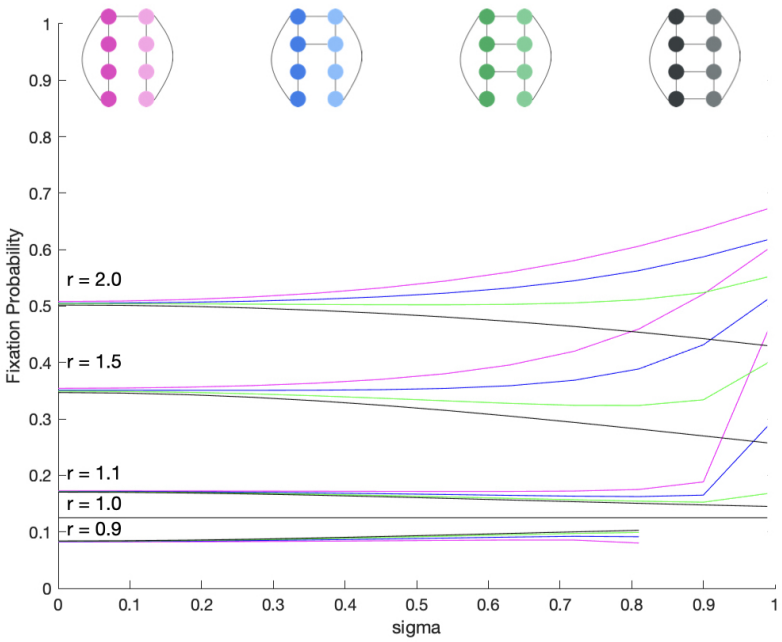

Figure A.4.2: Increasing Linear Inter-connectedness for 8-Node Two-Clique-Like Graph

This figure compares the singly-connected, doubly-connected, triply-connected, and n-connected two-clique-like graphs of 8 nodes across the various r values of 0.9, 1.0, 1.1, 1.5, and 2.0 and σ values from 0 to 0.99 (0.81 for $r = 0.81$). The pink, blue, green, and black lines represent the singly-connected, doubly-connected, triply-connected, and n-connected graphs respectively.

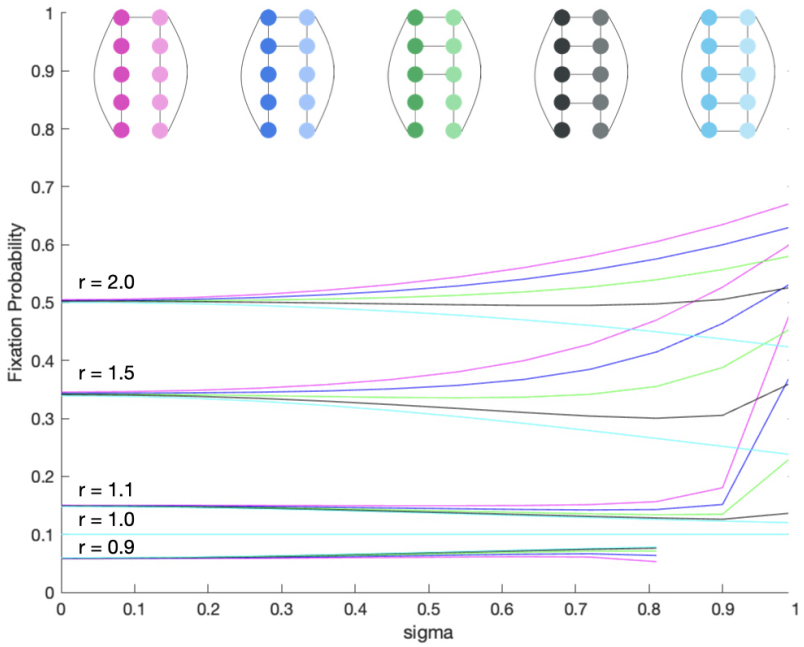

Figure A.4.3: Increasing Linear Inter-connectedness for 10-Node Two-Clique-Like Graph

This figure compares the singly-connected, doubly-connected, triply-connected, quad-connected, and n-connected two-clique-like graphs of 10 nodes across the various r values of 0.9, 1.0, 1.1, 1.5, and 2.0 and σ values from 0 to 0.99 (0.81 for $r = 0.81$). The pink, blue, green, black, and cyan lines represent the singly-connected, doubly-connected, triply-connected, quad-connected, and n-connected graphs respectively.

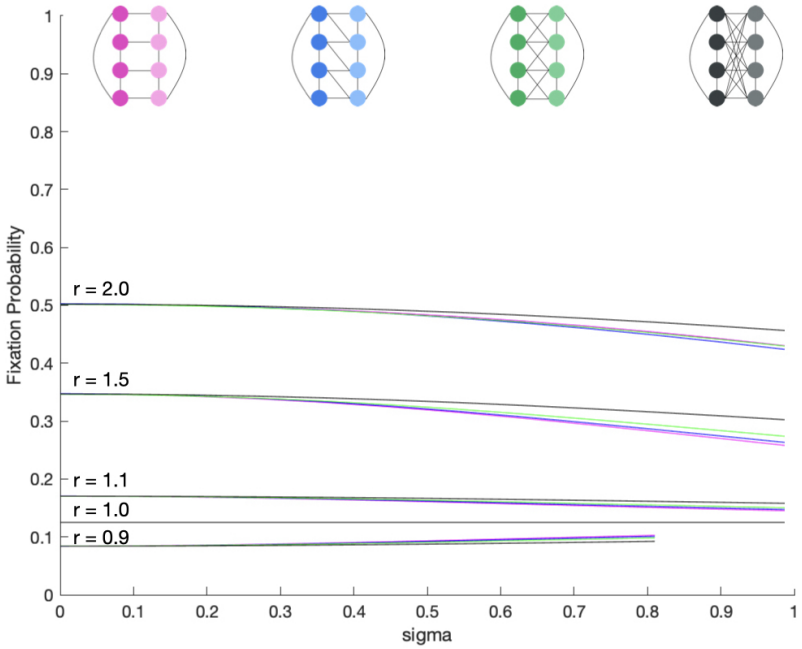

Figure A.4.4: Increasing Zig-Zag Inter-connectedness for Two-Clique-Like Graph

This figure compares the n-connected, zig-zag-connected, cross-connected, and completely-connected two-clique-like graphs of 8 nodes across the various r values of 0.9, 1.0, 1.1, 1.5, and 2.0 and σ values from 0 to 0.99 (0.81 for $r = 0.81$). The pink, blue, green, and black lines represent the n-connected, zig-zag-connected, cross-connected, and completely-connected graphs respectively.

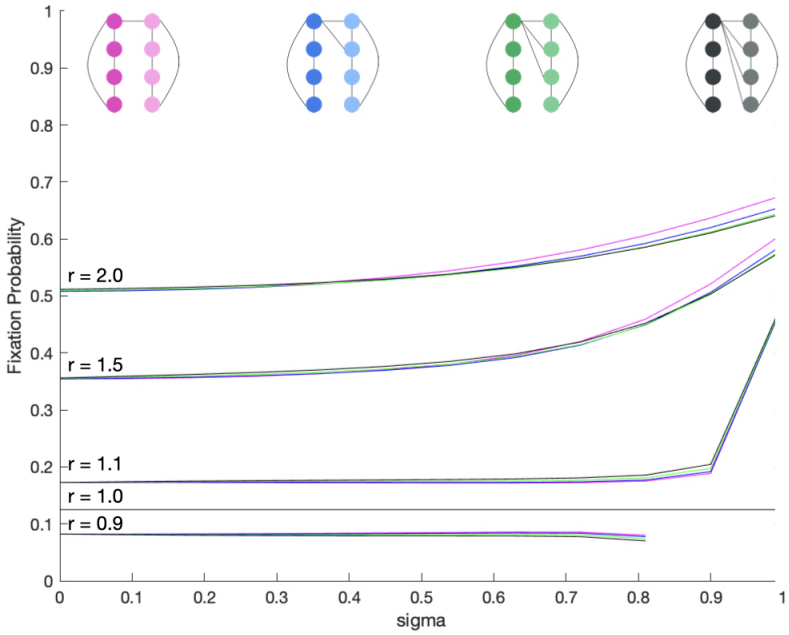

Figure A.4.5: Increasing Star Inter-connectedness for Two-Clique-Like Graph

This figure compares graphs with one, two, three, and four star-like inter-connected two-clique-like graphs of 8 nodes across the various r values of 0.9, 1.0, 1.1, 1.5, and 2.0 and σ values from 0 to 0.99 (0.81 for $r = 0.81$). The pink, blue, green, and black lines represent the graphs with one, two, three, and four between clique-like subgraph connections respectively.

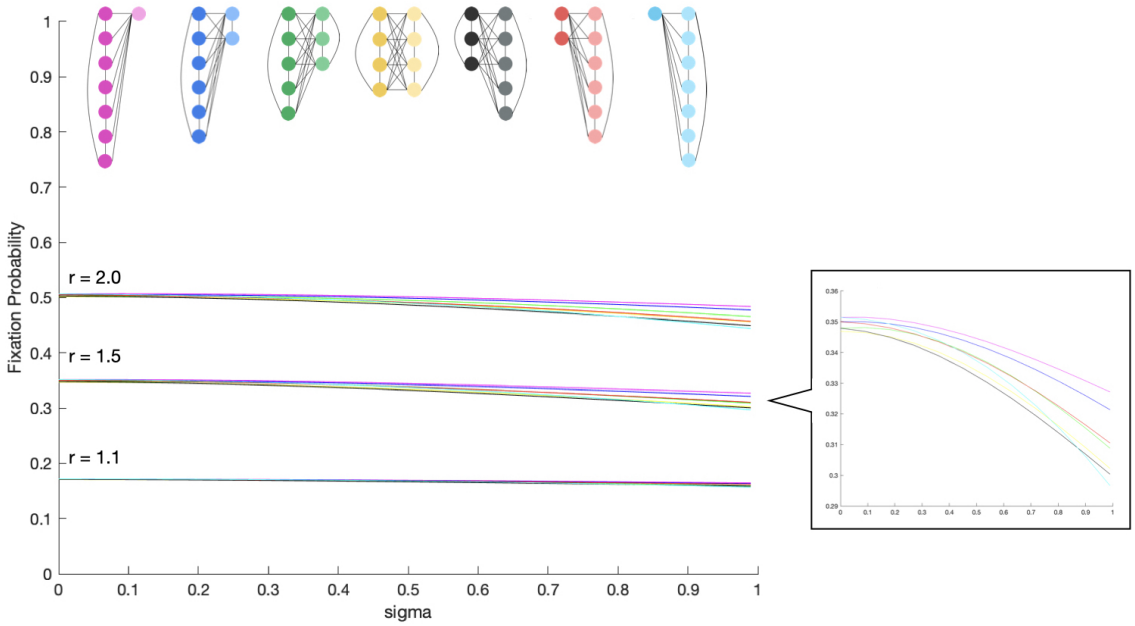

Figure A.4.6: Varying Island Sizes of Two-Clique-Like Graphs

This figure displays fixation probability for seven different graphs, six of which have unbalanced island sizes across σ value of 0 to 0.99 for r values 1.1, 1.5, and 2.0. Each line color corresponds to the colored graph displayed above. We note that in the calculation of these fixation probabilities, we keep the standard deviation of fitness constant at σ. However, because the number of green and red nodes changes across graph structures, to hold constant the overall standard deviation across graphs, we adjust the resulting deviation in red and green nodes for each graph as follows. For 1-7 or 7-1 structures, the single node has deviations of +/- $\sqrt{7} \cdot \sigma$, while the other seven nodes have deviations of +/- $\frac{\sqrt{7}}{7} \cdot \sigma$. For 2-6 or 6-2 structures, the isolated pair of nodes have deviations of +/- $\sqrt{3} \cdot \sigma$, while the other six nodes have deviations of +/- $\frac{\sqrt{3}}{3} \cdot \sigma$. Lastly, for 3-5 or 5-3 structures, the three nodes have deviations of +/- $\frac{\sqrt{15}}{3} \cdot \sigma$, while the other five nodes have deviations of +/- $\frac{\sqrt{15}}{5} \cdot \sigma$.

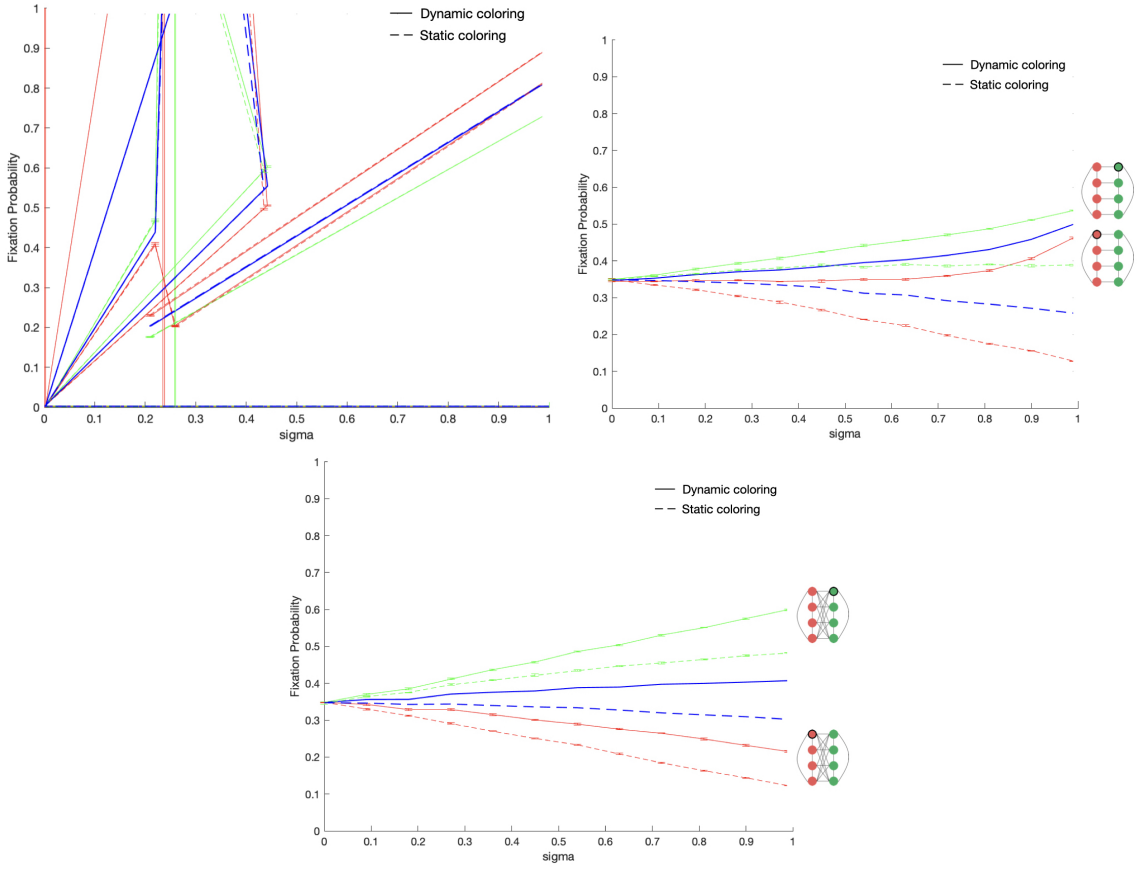

Figure A.4.7: Fixation Probability of Singly-Connected, N-Connected, Completely-Connected Two-Clique-Like Graph for Dynamic and Static Coloring

This figure displays the results of dynamic coloring on two-clique-like graphs, with $p = 0.25$, $m = 0.75$, and $r = 1.5$. The top-left panel corresponds to the singly-connected graph, the top-right panel corresponds to the n-connected graph, and the bottom-middle panel corresponds to the completely-connected graph. The bolded blue solid and dashed lines represent the average fixation probabilities, while the other colors represent different mutant initialization nodes, captured by the graph diagrams on the right. The top-left figure includes all eight initialization points due to a lack of symmetries in the singly-connected two-clique-like graph, and evidently has some zero fixation probabilities.